Modelling the onset of shear boundary layers in fibrous composite reinforcements by second gradient theory

Manuel Ferretti, Angela Madeo, Francesco Dell'Isola, Philippe Boisse

Modelling the onset of shear boundary layers in fibrous composite reinforcements by second gradient theory

Manuel Ferretti, Angela Madeo*, Francesco dell'Isola and Philippe Boisse

Abstract. It has been known since the pioneering works by Piola, Cosserat, Mindlin, Toupin, Eringen, Green, Rivlin and Germain that many micro-structural effects in mechanical systems can be still modeled by means of continuum theories. When needed, the displacement field must be complemented by additional kinematical descriptors, called sometimes microstructural fields. In this paper, a technologically important class of fibrous composite reinforcements is considered and their mechanical behavior is described at finite strains by means of a second gradient, hyperelastic, orthotropic continuum theory which is obtained as the limit case of a micromorphic theory. Following Mindlin and Eringen, we consider a micromorphic continuum theory based on an enriched kinematics constituted by the displacement field $\mathbf{u}$ and a second order tensor field $\boldsymbol{\psi}$ describing microscopic deformations. The governing equations in weak form are used to perform numerical simulations in which a bias extension test is reproduced. We show that second gradient energy terms allow for an effective prediction of the onset of internal shear boundary layers which are transition zones between two different shear deformation modes. The existence of these boundary layers cannot be described by a simple first gradient model and its features are related to second gradient material coefficients. The obtained numerical results, together with the available experimental evidences, allow us to estimate the order of magnitude of the introduced second gradient coefficients by inverse approach. This justifies the need of a novel measurement campaign aimed to estimate the value of the introduced second gradient parameters for a wide class of fibrous materials.

1. Introduction

In the engineering effort of designing new materials, a constant demand is directed towards the search for better performances and new functionalities. A class of materials which is gaining more and more attention is that of so-called complex materials, e.g. materials exhibiting different mechanical responses at different scales due to different scales of heterogeneity. Indeed, the overall mechanical behavior of such materials is macroscopically influenced by the underlying microstructure especially in presence of particular loading and/or boundary conditions. Therefore, understanding the mechanics of meso- and micro-structured materials is becoming a major issue in engineering.

Such materials may exhibit superior mechanical properties with respect to more commonly used engineering materials, also providing some advantages as easy formability processes. We focus in this paper on a class of engineering materials which are known as woven fibrous composite reinforcements. These materials are constituted by woven tows which are themselves made up of thousand of fibers. Different weaving schemes can be used giving rise to different types of composite reinforcements (see Fig.1), but in each of considered case one can assume that sharp changes in mechanical properties

The authors thank INSA-Lyon for the financial support assigned to the project BQR 2013-0054 "Matériaux Méso et Micro-Hétérogènes: Optimisation par Modèles de Second Gradient et Applications en Ingénierie".

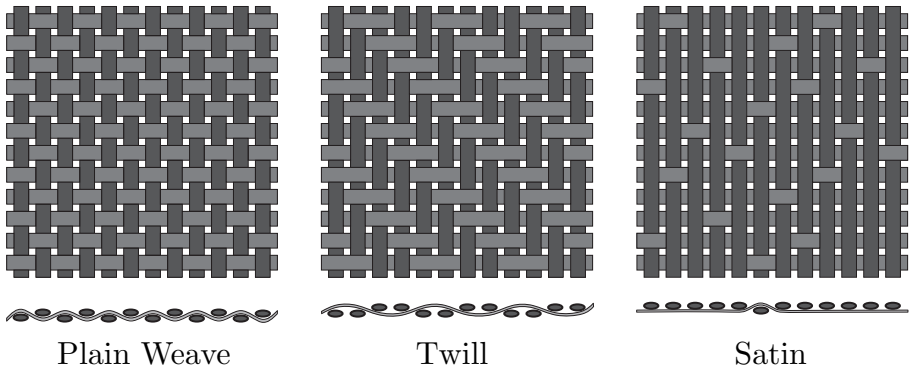

FIGURE 1. Schemes of weaving for fibrous composite reinforcements.

may occur inside the unit cell. Indeed, for the considered materials, the tensile stiffness of tows can be considered to be of many order of magnitudes higher than the shear stiffness related to angle variations between yarns. The hierarchical heterogeneity of composite reinforcements is illustrated in Fig. 2, in which three different scales can be recognized: the macroscopic scale (left), the mesoscopic scale (center) and the microscopic scale (right).

All materials are actually heterogeneous if one considers sufficiently small scales, but the woven composites reinforcements show their heterogeneity at scales which are significant from an engineering point of view. It is also clear that woven materials also macroscopically show strong anisotropy, since their mechanical response significantly varies if the load is applied in the direction of the fibers or in some other direction. As it will be better pointed out in the following, the introduced continuum model for composite reinforcements belongs to the class of initially orthotropic continua, i.e. continua which have two privileged directions in their undeformed configuration.

The fibrous composite preforms can be shaped and their final shape is maintained by injection and curing of a thermoset resin or by the use of a thermoplastic polymer. The final composite material commonly used in aerospace engineering is hence constituted by the fibrous composite reinforcement and the organic matrix. We are interested in this paper only in describing the mechanical behavior of the fibrous composite reinforcements since this knowledge is fundamental for the process of formability of the final composite. Following [13, 14] we find convenient to model the quoted fibrous reinforcements as continuous media. This hypothesis can be considered to be realistic if no relative displacement between superimposed fibers occurs. In other words, we are assuming that two superimposed fibers can rotate around their contact point, while no slipping takes place. This hypothesis is generally verified during experimental analyses, even at finite strains. In fact, when straight lines are drawn on the textile reinforcement, these lines become curved after forming but they remain continuous (see e.g. [10]). As it will be better pointed out in the remainder of this paper, the anisotropy of the considered reinforcements will be taken into account by introducing suitable hyperelastic, orthotropic constitutive laws which are able to characterize the behavior of considered materials also at large strains.

Nevertheless, a first gradient continuum orthotropic model is not able to take into account all the possible effects that the microstructure of considered materials have on their macroscopic deformation. More precisely, some particular loading conditions, associated to particular types of boundary conditions may cause some microstructure-related deformation modes which are not fully taken into account in first gradient continuum theories. This is the case, for example, when observing some regions inside the materials in which high gradients of deformation occur, concentrated in those relatively narrow regions which we will call boundary layers.

Actually, the onset of shear boundary layers can be observed in some experimental tests which are used to characterize the mechanical properties of fibrous composite reinforcements. Indeed, internal boundary layers do arise in the so-called bias extension test, the phenomenology of which we duly

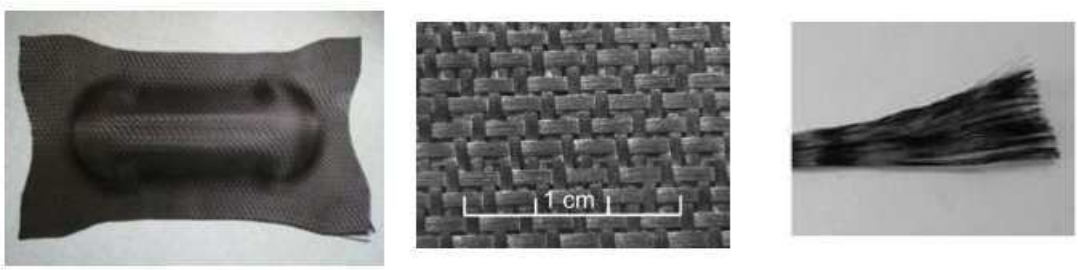

FIGURE 2. The different scales of textile composite reinforcements.

describe in section 4. One way to deal with the description of such boundary layers, while remaining in the framework of a macroscopic theory, is to consider so-called "generalized continuum theories". Such generalized theories allow for the introduction of a class of internal actions which is wider than the one which is accounted for by classical first gradient Cauchy continuum theory. These more general contact actions excite additional deformation modes which can be seen to be directly related with the properties of the microstructure of considered materials.

Indeed, it has been known since the pioneering works by Piola [67], Cosserat [15], Midlin [57], Toupin [86], Eringen [29], Green and Rivlin [37] and Germain [35, 36] that many microstructure-related effects in mechanical systems can be still modeled by means of continuum theories. It is known since then that, when needed, the placement function must be complemented by additional kinematical descriptors, called sometimes micro-structural fields. More recently, these generalized continuum theories have been widely developed to describe the mechanical behavior of many complex systems, such as e.g. porous media [53, 80, 78, 22], capillary fluids [12, 16, 17, 20, 18], exotic media obtained by homogenization of heterogeneous media [3, 81, 66]. Interesting applications on wave propagation in such generalized media has also gained attention in the recent years for the possible application of this kind of materials to passive control of vibrations and stealth technology (see e.g. [24, 54, 68, 76]).

In this paper, the class of fibrous composite preforms described before is considered and their macroscopic mechanical behavior (i.e. at a scale relatively larger than the yarn) is described by means of a second gradient, hyperelastic continuum theory. The quoted hyperelastic, second gradient theory is obtained as the limit case of a micromorphic theory, following what done in [7, 57] for the linear-elastic case. The governing equations in weak form are used as a basis for the formulation of suitable numerical codes, which allow to perform simulations reproducing the so-called bias extension test. We show that second gradient energy terms allow for an effective prediction of the onset of internal shear boundary layers which can be defined as those transition zones between two different regions exhibiting different shear deformation modes. The existence and thickness of these boundary layers cannot be described by a first gradient model and its overall features are related to the particular second gradient model introduced in this paper. The obtained numerical results seem to be in a good agreement with the already available experimental evidence and fully justify the need of a novel measurement campaign.

2. Micromorphic media and second gradient continua

We describe the deformation of the considered continuum by introducing a Lagrangian configuration $B_L \subset \mathbb{R}^3$ and a suitably regular kinematical field $\boldsymbol{\chi}(\mathbf{X}, t)$ which associates to any material point $\mathbf{X} \in B_L$ its current position $\mathbf{x}$ at time t. The image of the function $\boldsymbol{\chi}$ gives, at any instant t the current shape of the body $B_E(t)$: this time-varying domain is usually referred to as the Eulerian configuration of the medium and, indeed, it represents the system during its deformation. Since we will use it in the following, we also introduce the displacement field $\mathbf{u}(\mathbf{X}, t) := \boldsymbol{\chi}(\mathbf{X}, t) - \mathbf{X}$, the

tensor $\mathbf{F} := \nabla\boldsymbol{\chi}$ and the Right Cauchy-Green deformation tensor[1] $\mathbf{C} := \mathbf{F}^T \cdot \mathbf{F}$. The kinematics of the continuum is then enriched by adding a second order tensor field $\boldsymbol{\psi}(\mathbf{X}, t)$ which accounts for deformations associated to the microstructure of the continuum. Indeed, as it was explained e. g. by Mindlin [57] and Cosserat [15], the addition of supplementary kinematical fields can be of help to describe the deformation of the microstructure of the considered material independently of its average continuum deformation. If, on the one hand, Cosserat's models are able to complement the classical continuum deformations with extra rotations of considered microstructure, on the other hand, micromorphic models of the type considered in this paper also allow to consider micro-stretches and micro-shear deformations. In particular, the introduced micromorphic tensor $\boldsymbol{\psi}(\mathbf{X}, t)$ allows to account for all these microscopic deformation in a very general fashion. If some constraints are introduced on the tensor $\boldsymbol{\psi}$, the micromorphic model can then be particularized so as to obtain Cosserat or second gradient models as limit cases. In what follows, the current state of the considered medium is, in general, identified by 12 independent kinematical fields: 3 components of the displacement field and 9 components of the micro-deformation field. Such a theory of a continuum with microstructure has been derived in [57] for the linear-elastic case and re-proposed e.g. in [30, 31, 32, 33] for the case of non-linear elasticity. For the sake of clearness, using similar notations to [57] and [7], we introduce the following kinematical quantities which are all functions of the basic kinematical fields introduced before

$$\begin{aligned} &\varepsilon_{ij} = (C_{ij} - \delta_{ij})/2, && \text{the macro-strain,} \\ &\gamma_{ij} = \varepsilon_{ij} - \psi_{ij}, && \text{the relative(micro/macro) deformation,} \\ &\kappa_{ijk} = \psi_{ij,k}, && \text{the gradient of micro-deformation,} \end{aligned} \tag{1}$$

where clearly C_{ij} and ψ_{ij} represent the components of the second order tensors $\mathbf{C}$ and $\boldsymbol{\psi}$ respectively. If one, for example, imposes the relative deformation to be zero (i.e. $\psi_{ij} \to \varepsilon_{ij}$), then $\kappa_{ijk} \to \varepsilon_{ij,k}$ and one recovers the standard second gradient theory presented in [35, 36]. As it will be more clearly explained in the following, the external actions which can be introduced in the framework of a micromorphic continuum theory are more easily understandable than those intervening in second gradient theories since they have a more direct physical meaning. Since second gradient theory can be readily obtained as limit case of the micromorphic theory, one can then derive the second gradient contact actions in terms of the micromorphic ones following the procedure used in [7]. We present in the following the weak formulation of a constrained micromorphic theory which will actually give rise to a particular second gradient theory. This constrained micromorphic theory is the one which we directly implement in the numerical simulations presented in this paper.

2.1. Equations in weak form for a constrained micromorphic continuum

We assume that we can write the power of internal actions as the first variation of a suitable action functional $\mathcal{A}$ as follows

$$\mathcal{P}^{int} = \delta\mathcal{A} = \delta \int_{B_L} \left[W\left(\varepsilon_{ij},\, \gamma_{ij},\, \kappa_{ijk}\right) + \sum_{\alpha=1}^{n} \lambda_\alpha\, f_\alpha(\varepsilon_{ij},\, \gamma_{ij},\, \kappa_{ijk}) \right] d\mathbf{X}, \tag{2}$$

where W and f are real scalar-valued functions of the introduced deformation measures and, in particular, $W\left(\varepsilon_{ij},\, \gamma_{ij},\, \kappa_{ijk}\right)$ is the bulk micromorphic strain energy density, λ_α are Lagrange multipliers and f_α are particular constraints the particular form of which will be better specified later on. As it will be better explained in the sequel, this expression of the power of internal forces is the one which is necessary to describe a micromorphic continuum which is subjected to the n constraints $f_\alpha(\varepsilon_{ij},\, \gamma_{ij},\, \kappa_{ijk}) = 0$.

[1]Here in the sequel a central dot indicates simple contraction between tensors of order greater than zero. For example if $\mathbf{A}$ and $\mathbf{B}$ are second order tensors of components A_{ij} and B_{jh} respectively, then $(\mathbf{A} \cdot \mathbf{B})_{ih} := A_{ij}B_{jh}$, where Einstein notation of sum over repeated indeces is used.

Considering that the independent kinematical fields appearing in (2) are indeed ε_{ij}, ψ_{ij} and κ_{ijk}, it can be recovered that the power of internal actions can be rewritten by computing the first variation of the action functional as

$$\mathcal{P}^{int} = \delta\mathcal{A} = \int_{B_L} \left(\frac{\partial W}{\partial \varepsilon_{ij}} + \sum_{\alpha=1}^{n} \lambda_\alpha \frac{\partial f_\alpha}{\partial \varepsilon_{ij}} \right) \delta\varepsilon_{ij} + \left(\frac{\partial W}{\partial \psi_{ij}} + \sum_{\alpha=1}^{n} \lambda_\alpha \frac{\partial f_\alpha}{\partial \psi_{ij}} \right) \delta\psi_{ij} + \left(\frac{\partial W}{\partial \kappa_{ijk}} + \sum_{\alpha=1}^{n} \lambda_\alpha \frac{\partial f_\alpha}{\partial \kappa_{ijk}} \right) \delta\kappa_{ijk} + \sum_{\alpha=1}^{n} f_\alpha \delta\lambda_\alpha, \tag{3}$$

where from now on we drop the symbol $d\mathbf{X}$ inside the integral sign and we adopt the Einstein notation of sum over repeated indices if no confusion can arise.

As for the expression of the power of external forces, we assume that they take the following general form (see also [57, 7])

$$\mathcal{P}^{ext} = \int_{B_L} b_i^{ext} \delta u_i + \int_{B_L} \Phi_{ij}^{ext} \delta\psi_{ij} + \int_{\partial B_L} t_i^{ext} \delta u_i + \int_{\partial B_L} T_{ij}^{ext} \, \delta\psi_{ij} \tag{4}$$

where b_i^{ext} are volume forces, Φ_{ij} are so called double forces per unit volume, t_i^{ext} are forces per unit area and T_{ij}^{ext} are double forces per unit area. The physical meaning of aforementioned external actions is immediate: b_i^{ext} and t_i^{ext} work on the displacement of the centroid of each Representative Elementary Volume, while Φ_{ij}^{ext} and T_{ij}^{ext} work on micro-deformations inside the considered REV. If one forces $\psi_{ij} \to \varepsilon_{ij}$, i.e. imposes the constraint $\psi_{ij} - \varepsilon_{ij} = 0$, then a more complicated form of the contact actions than those appearing in (4) can be derived by integration by parts. In this way, it is possible to recover the standard form for external actions of second gradient materials which work on displacement and on the normal derivatives of displacement (see e.g. [35, 51, 79, 52, 19, 21, 25]). Considering the surface power densities $t_i^{ext}\delta u_i$ and $T_{ij}^{ext}\delta\psi_{ij}$ appearing in expression (4) for the power of external actions, one can imagine to act on the boundary of considered body both by assigning the forces and/or double forces (natural boundary conditions) or by assigning the displacements and/or micro-deformation (kinematical boundary conditions).

The mechanical governing equations in weak form can be directly expressed by imposing the validity of the principle of virtual powers

$$\mathcal{P}^{int} = \mathcal{P}^{ext}, \tag{5}$$

where $\mathcal{P}^{int}$ and $\mathcal{P}^{ext}$ are respectively given in Eq. (3) and (4). We explicitly remark that, given the considered expression of the principle of virtual powers, we are assuming that the considered phenomena are sufficiently slow to neglect inertia. We do not explicitly write here the corresponding strong form of balance equations since we will directly implement a particularization of the weak form (5) in the finite element code used to perform numerical simulations.

3. Hyperelastic orthotropic model with micromorphic correction

In this section we specify the constitutive equations for the strain energy density $W\left(\varepsilon_{ij},\, \gamma_{ij},\, \kappa_{ijk}\right)$ which we use to model the mechanical behavior of some fibrous composite reinforcements in the finite strain regime. We will equivalently use the deformation measure $\mathbf{C} = 2\boldsymbol{\varepsilon} + \mathbf{I}$ instead of $\boldsymbol{\varepsilon}$ to specify the form for the energy, i.e. $W\left(\varepsilon_{ij},\, \gamma_{ij},\, \kappa_{ijk}\right) = \tilde{W}\left(C_{ij},\, \gamma_{ij},\, \kappa_{ijk}\right)$. In particular, we will assume that

$$\tilde{W}\left(C_{ij},\, \gamma_{ij},\, \kappa_{ijk}\right) = W_I(C_{ij}) + W_{II}(\kappa_{ijk}). \tag{6}$$

In this formula W_I is the first gradient strain energy and W_{II} is the energy associated to the macro-inhomogeneity of micro-deformation. We do not explicitly consider a coupling energy depending on γ_{ij}, but some coupling effects will be accounted for by introducing particular constraints $f_\alpha(\varepsilon_{ij}, \gamma_{ij}, \kappa_{ijk}) = 0$ in the power of internal actions by using Lagrange multipliers, as specified in Eq.(2).

3.1. Representation theorem for hyperelastic orthotropic materials

Various hyperelastic constitutive equations for an isotropic strain energy density $W^{iso}(\mathbf{C})$ have been proposed in the literature which are suitable to describe the mechanical behavior of isotropic materials even at finite strains (see e.g. [61, 84]). Generalized constitutive laws are also available for linear elastic isotropic second gradient media (see [23]). These constitutive equations for isotropic materials are classically derived starting from a well-known representation theorem for the strain energy potential which states that only three independent scalar invariants of the Cauchy-Green tensor $\mathbf{C}$ are sufficient to correctly represent the functional dependence of W^{iso} on $\mathbf{C}$. In other words, for an isotropic material, it is sufficient to consider that $W^{iso}(\mathbf{C}) = W(i_1, i_2, i_3)$, where $i_1,\ i_2,\ i_3$ are the three scalar invariants of $\mathbf{C}$ classically defined as

$$i_1 = \mathrm{tr}(\mathbf{C}), \quad i_2 = \mathrm{tr}\left(\det(\mathbf{C})\ \mathbf{C}^{-\mathbf{T}}\right), \quad i_3 = \det(\mathbf{C}).$$

These three invariants respectively describe local deformations associated to changes of length, changes of area and changes of volume: superposition of these three deformation modes are sufficient to reproduce the global deformation of an isotropic medium. Constitutive equations for transversely isotropic materials are also well assessed in the literature (see e.g. [44, 8, 9, 62, 13, 45]) and their derivation relies on the classical representation theorem according to which five independent invariants of the tensor $\mathbf{C}$ are needed to characterize the behavior of such materials: $W^{tran}(\mathbf{C}) = W(i_1, i_2, i_3, i_4, i_5)$. If one denotes by $\mathbf{m}_1$ the unitary vector along the preferred direction inside the transversely isotropic material in its reference (Lagrangian) configuration, then the two additional invariants appearing in the representation of W^{tran} are defined as

$$i_4 = \mathbf{m}_1 \cdot \mathbf{C} \cdot \mathbf{m}_1, \quad i_5 = \mathbf{m}_1 \cdot \mathbf{C}^2 \cdot \mathbf{m}_1.$$

These two invariants respectively describe local stretch in the direction of the preferential direction $\mathbf{m}_1$ and changes of angles mixed to changes of length.

As far as orthotropic materials are considered, clear and exploitable constitutive hyperelastic equations are harder to be found in the literature. Plenty of authors try to generalize the representation theorems valid for isotropic and transversely isotropic media, but often there is apparently not agreement between the different versions proposed for such a theorem. The more diffused version of the representation theorem for the strain energy potential for orthotropic media states that seven invariants can be used to write the functional dependence of the strain energy density (see e.g. [43, 82, 62]). More precisely, denoting by $\mathbf{m}_1$ and $\mathbf{m}_2$ two orthogonal unitary vectors along the preferred directions in the considered orthotropic material, the functional dependence of the orthotropic energy on $\mathbf{C}$ can be expressed in the form $W^{orth} = W(i_1, i_2, i_3, i_4, i_5, i_6, i_7)$, where the additional two invariants are defined as

$$i_6 = \mathbf{m}_2 \cdot \mathbf{C} \cdot \mathbf{m}_2, \quad i_7 = \mathbf{m}_2 \cdot \mathbf{C}^2 \cdot \mathbf{m}_2,$$

Nevertheless, it can be proved that, indeed, only six independent scalar invariants are sufficient to completely describe the behavior of an orthotropic material (see the elegant proof given in [69]), so that, even if it is effectively possible to write the strain energy as function of seven scalar invariants, it must be kept in mind that not all of them are truly independent functions of $\mathbf{C}$. In particular, following [69], one can think to introduce the following set of six invariants to represent the functional dependence of W on $\mathbf{C}$:

$$i_O := \{i_1, i_4, i_6, i_8, i_9, i_{10}\},$$

where all the invariants not previously defined are given by

$$i_8 = \mathbf{m}_1 \cdot \mathbf{C} \cdot \mathbf{m}_2, \quad i_9 = \mathbf{m}_1 \cdot \mathbf{C} \cdot \mathbf{m}_3, \quad i_{10} = \mathbf{m}_2 \cdot \mathbf{C} \cdot \mathbf{m}_3,$$

where $\mathbf{m}_3 := \mathbf{m}_1 \wedge \mathbf{m}_2$. All the invariants belonging to the set i_O correspond to simple deformation modes. In particular, in addition to the invariants already discussed before, one can remark that i_6 represents stretching in the direction $\mathbf{m}_2$, while i_8, i_9 and i_{10} represent changes of angles between the

directions $(\mathbf{m}_1, \mathbf{m}_2)$, $(\mathbf{m}_1, \mathbf{m}_3)$ and $(\mathbf{m}_2, \mathbf{m}_3)$ respectively. It can be shown (see [69]) that all previously introduced invariants can be written as functions of the six invariants in i_O as

$$\begin{aligned} i_2 &= i_4 i_6 + (i_4 + i_6)\,(i_1 - (i_4 + i_6)) - i_8^2 - i_9^2 - i_{10}^2, \\ i_3 &= \left(i_4 i_6 - i_8^2\right)(i_1 - (i_4 + i_6)) + 2\; i_8 i_9 i_{10} - i_6 i_9^2 - i_4 i_{10}^2, \\ i_5 &= i_4^2 + i_8^2 + i_9^2, \qquad i_7 = i_6^2 + i_8^2 + i_{10}^2. \end{aligned}$$

The fact of correctly identifying the maximum number of scalar invariants which are all independent functions of $\mathbf{C}$ is of fundamental importance when one wants to write the constitutive hyperelastic laws starting from the considered strain energy potential. Indeed, a hyperelastic energy is, by construction, differentiable with respect to the strain tensor $\mathbf{C}$ and, considered that all the invariants in i_O are independent functions of $\mathbf{C}$, one can obtain the second Piola-Kirchhoff stress tensor for orthotropic materials as

$$\mathbf{S} := \frac{\partial W^{orth}}{\partial \boldsymbol{\varepsilon}} = 2\frac{\partial W^{orth}}{\partial \mathbf{C}} = 2\sum_{k \in i_O} \frac{\partial W^{orth}}{\partial i_k}\,\frac{\partial i_k}{\partial \mathbf{C}}, \tag{7}$$

$$W^{orth}(\mathbf{C}) := W(i_1, i_4, i_6, i_8, i_9, i_{10}) \tag{8}$$

In [69] it is also explicitly proved that a strain energy $\bar{W}(i_1, i_2, i_3, i_4, i_5, i_6, i_7)$ which is function of the seven classical invariants can also be obtained starting from the strain energy W^{orth} defined in (8). If we consider the functional dependence of W^{orth} on the six invariants in i_O given in (8) we must take into account the results found in [69] where it is proven that $W(i_1, i_4, i_6, i_8, i_9, i_{10}) = \bar{W}\left(i_1, i_4, i_6, |i_8|, |i_9|, |i_{10}|, sgn(i_8 i_9 i_{10})\right)$. Using this expression for the energy and replacing it in (7), then it is possible to prove that the constitutive law for the second Piola Kirchhoff stress tensor is given by

$$\begin{aligned} \mathbf{S} = {} & 2\frac{\partial \bar{W}}{\partial i_1}\mathbf{I} + 2\frac{\partial \bar{W}}{\partial i_4}\mathbf{m}_1 \otimes \mathbf{m}_1 + 2\frac{\partial \bar{W}}{\partial i_6}\mathbf{m}_2 \otimes \mathbf{m}_2 + sgn(i_8)\frac{\partial \bar{W}}{\partial |i_8|}(\mathbf{m}_1 \otimes \mathbf{m}_2 + \mathbf{m}_2 \otimes \mathbf{m}_1) \\ & + sgn(i_9)\frac{\partial \bar{W}}{\partial |i_9|}(\mathbf{m}_1 \otimes \mathbf{m}_3 + \mathbf{m}_3 \otimes \mathbf{m}_1) + sgn(i_{10})\frac{\partial \bar{W}}{\partial |i_{10}|}(\mathbf{m}_2 \otimes \mathbf{m}_3 + \mathbf{m}_3 \otimes \mathbf{m}_2). \end{aligned} \tag{9}$$

This orthotropic constitutive law can be used to model the macroscopic behavior at finite strains of 3D interlocks of fibrous composite reinforcements. Fully reliable models which are able to describe the mechanical behavior of 3D composite preforms are not completely developed up to now both for the interlock reinforcements (see e.g. [14]) and for the complete composite (reinforcements plus organic matrix) (see e.g. [26]). For this reason, the mechanical characterization of such materials is nowadays a major scientific and technological issue. The mechanical behavior of composite preforms with rigid organic matrix (see e.g. [26, 65, 55, 56]) is quite different from the behavior of the sole fibrous reinforcements (see e.g. [14]). In [14] a hyperelastic approach is presented which allows to capture the main features of 3D interlocks at finite strain. On the other hand, in [14] it is also underlined that Cauchy continuum theory may not be sufficient to model a class of complex contact interactions which are related to local stiffness of the yarns and which macroscopically affect the overall deformation of interlocks. Such microstructure-related contact interactions may be taken into account by using generalized continuum theories, such as higher order or micromorphic theories. In this paper we will limit ourselves to the application of a hyperelastic, orthotropic, second gradient model to the case of thin fibrous composite reinforcements at finite strains, for which the third direction can easily be thought to have negligible effect on the overall behavior of the material.

3.2. Phenomenological choice of the potential W^I for thin sheets of fibrous composite reinforcements

Explicit expressions for the strain energy potential W^{orth} as function of the invariants i_O which are suitable to describe the real behavior of orthotropic elastic materials are difficult to be found in

the literature. Certain constitutive models are for instance presented in [44], where some polyconvex energies for orthotropic materials are proposed to describe the deformation of rubbers in uniaxial tests. Explicit anisotropic hyperelastic potentials for soft biological tissues are also proposed in [42] and reconsidered in [77, 6] in which their polyconvex approximations are derived. Other examples of polyconvex energies for anisotropic solids are given in [85].

Polyconvex energies are energies automatically satisfying the Legendre-Hadamard (L-H) ellipticity condition which, in turns, guarantees material stability of considered potentials. Reliable constitutive models for the description of the real behavior of fibrous composite reinforcements at finite strains are even more difficult to be found in the literature and can be for instance recovered in [2, 13]. In the present paper, we will introduce a first gradient anisotropic hyperelastic potential of the type proposed in [13, 14] to model the overall behavior of considered fibrous materials and we will add a second gradient term to account for the onset of some boundary layers which are observed experimentally but which cannot be described by means of a first gradient theory. We do not attempt in this paper to test L-H ellipticity of the chosen first gradient potential $W_I(C_{ij})$, our major concern being that one of recovering the experimental deformed shape of some particular fibrous composite preforms. We are nevertheless aware that the used first gradient potential might not be L-H elliptic on some precise directions along which one could hence obtain material instability. We postpone these investigations to subsequent works in which we will also put in evidence how the addition of some second gradient terms in the energy potential can indeed guarantee mathematical existence of the solution.

To the sake of consistency, we recall here some steps which have been followed to derive the constitutive hyperelastic expression for the potential $W_{\mathrm{I}}(\mathbf{C})$ proposed in [13, 14]. We recall that the two privileged directions in the reference (or Lagrangian) configuration are identified by means of two vectors $\mathbf{m}_1$ and $\mathbf{m}_2$ which are assumed to be orthogonal and to have unitary length. For the considered fibrous composite reinforcements the two privileged directions clearly coincide with the fiber directions $\mathbf{m}_1$ and $\mathbf{m}_2$ (called warp and weft) in the undeformed configuration. For the case studied in this paper, we focus on the modeling of specimens of fibrous composite reinforcements which are very thin in the direction $\mathbf{m}_3 = \mathbf{m}_1 \wedge \mathbf{m}_2$ and we will treat the case of thick composite reinforcements in subsequent works. The fact of considering very thin sheets of fibrous composite preforms allows us to assume that the strain energy potential is constant with respect to the invariants i_9 and i_{10}, so that the calculation to get the stress tensor $\mathbf{S}$ starting from (7) results to be simplified since the last two terms are automatically vanishing. We hence propose the following additive decomposition which separately accounts for the potential associated to isotropic deformation, to elongation of fibers in the two privileged directions (warp and weft) and to the variation of the shear angle among two fibers respectively

$$W_{\mathrm{I}}(\mathbf{C}) = W^{NH}(\mathbf{C}) + W^{1}_{\mathrm{elong}}(\mathbf{C}) + W^{2}_{\mathrm{elong}}(\mathbf{C}) + W_{\mathrm{shear}}(\mathbf{C}). \tag{10}$$

The isotropic energy potential W^{NH} can be assumed to take the classical Neo-Hooke form

$$W^{NH}(i_1, i_4, i_6, i_8, i_9, i_{10}) = \mu\left[(i_1 - 3) - ln\left(i_3(i_1, i_4, i_6, i_8, i_9, i_{10})\right)\right],$$

where the explicit expression of i_3 as function of the other invariants is given in the previous subsection. We remark that, in the case studied in the following, the isotropic deformations can be considered to be very small compared to the anisotropic ones, so that the stiffness coefficient μ will be considered to be very small with respect to the anisotropic material constants. As for the anisotropic energies appearing in (10), we now specify their explicit dependence on the invariants i_4, i_6 and i_8 following what done in [14]. To do so, we first introduce the three scalar functions

$$I^{1}_{elong}(i_4) = ln\left(\sqrt{i_4}\right), \qquad I^{2}_{elong}(i_6) = ln\left(\sqrt{i_6}\right), \qquad I_{shear}(i_4, i_6, i_8) = \frac{i_8}{\sqrt{i_4 i_6}},$$

which clearly represent elongation measures in the two principal directions of fibers and variation of the angle between fibers. It can be checked that the function I_{shear} is indeed related to the angle variation ϕ from the reference angle between the fibers by the formula $I_{shear} = sin(\phi)$ (see e.g.[13, 14]). We then recall the explicit form of the three introduced potentials which has been shown to be suitable

for describing physically reasonable material behavior for thin fibrous composite reinforcements (see [13, 14]):

$$
\begin{aligned}
W^1_{\rm elong}\left(i_1\right) &= \begin{cases} \frac{1}{2}\mathrm{K}^0_{\rm elong}\left(I^1_{\rm elong}\right)^2 & \text{if } I^1_{\rm elong} \leq I^0_{\rm elong} \\ \frac{1}{2}\mathrm{K}^1_{\rm elong}\left(I^1_{\rm elong}-I^0_{\rm elong}\right)^2 + \frac{1}{2}\mathrm{K}^0_{\rm elong}I^1_{\rm elong}I^0_{\rm elong} & \text{if } I^1_{\rm elong} > I^0_{\rm elong}, \end{cases} \\
W^2_{\rm elong}\left(i_2\right) &= \begin{cases} \frac{1}{2}\mathrm{K}^0_{\rm elong}\left(I^2_{\rm elong}\right)^2 & \text{if } I^2_{\rm elong} \leq I^0_{\rm elong} \\ \frac{1}{2}\mathrm{K}^1_{\rm elong}\left(I^2_{\rm elong}-I^0_{\rm elong}\right)^2 + \frac{1}{2}\mathrm{K}^0_{\rm elong}I^2_{\rm elong}I^0_{\rm elong} & \text{if } I^2_{\rm elong} > I^0_{\rm elong}, \end{cases} \\
W_{\rm shear}\left(i_4,i_6,|i_8|\right) &= \begin{cases} \mathrm{K}^{12}_{\rm shear}\left(|I_{\rm shear}|\right)^2 & \text{if } |I_{\rm shear}| \leq I^0_{\rm shear} \\ \mathrm{K}^{21}_{\rm shear}\left(1-|I_{\rm shear}|\right)^{-p} + W^0_{\rm shear} & \text{if } |I_{\rm shear}| > I^0_{\rm shear}. \end{cases}
\end{aligned}
\tag{11}
$$

In the three proposed potentials one can notice the existence of threshold values of the three introduced scalar functions, namely I^0_{elong} for I^1_{elong} and I^2_{elong} and I^0_{shear} for I_{shear}. The threshold value for the elongation strain measures I^0_{elong} is due to the fact that, for small stretch of the fibers, the weft and warp yarns are undulated due to weaving. When the fibers are completely stretched, they start showing their complete tension stiffness which can indeed reach extremely high values if one considers e.g. carbon fibers. Also for the shear deformation measure a threshold value is identified (related to lateral contact between the yarns due to shearing) which discriminates between two different behaviors.

As already explained in detail, the first gradient energy given by Eqs. (10), (11) has been introduced on a phenomenological basis. The strong non-linearities and some loss of regularity of such energy make the well-posedness of elastic problems related to it difficult to prove. Actually, (see [60]) some new mathematical results seem to be needed in order to regularize the considered form of the energy potential. In the literature, these regularization has been proposed by the use of judicious numerical techniques: in [38, 39] the functional space where looking for solutions is constrained by suitably choosing the mesh for employed finite elements. This is done in [38, 39] in conformity with the indications given by the models developed e.g. in [82]. Another possible method for regularizing hill-posed problems, as the one which seems to be confronted here, is to introduce an *ad hoc* regularizing parameters involving higher order derivatives or fictitious additional kinematical parameters. However, until a physical interpretation for such parameters is not reached, one cannot consider that the ill-posedness is removed: indeed, as it is obvious, there is not a unique limit of the solution when these parameters vanish. An elegant example of successful regularization, obtained by introducing in the mathematical modeling some physically relevant corrections, is given e.g. in [46] where some important dissipation phenomena in strain softening are accounted for by means of suitably chosen regularizing parameters. It has to be remarked that the first remedy proposed by [38, 39] determines the correct limit to be obtained when regularizing parameters vanish. In the subsequent subsection we propose a first attempt to find a regularized energy which is based on the physical concept of longer range mechanical interactions among non-adjacent unit cells of considered fibrous composite reinforcements. A validation of the regularized model proposed in the present paper is obtained by comparing the numerical results presented here with those obtained in [38, 39].

Mathematically speaking, micromorphic models produce boundary problems for partial differential equations which are "singular perturbations" of the boundary problems obtained in the framework of first gradient models. Therefore, the type of PDEs may change when micromorphic constitutive parameters tend to zero and, as a consequence, it could be lost the possibility of describing the onset of boundary layers. Also relevant are the phenomena of loss of stability, buckling and post-buckling phenomena which may occur in considered structures: while refraining here to attempt to model e.g. the wrinkling occurring in bias test for very high imposed displacements, we want to mention that, by using methods similar to those presented in [48, 49, 50], also this modeling challenge may be confronted.

3.3. Some physical considerations leading to regularized micromorphic strain energy potentials

In woven reinforcements for composite materials, when the external loads are applied only at the terminal extremities of the yarns, a unit cell is deformed because of its interaction with the closest ones. The basic assumption about these interactions which leads to first gradient homogenized continua is that they are negligible when the two considered cells are not the closest adjacent ones. However, simple mechanical considerations can be heuristically developed: i) for low loads, friction among yarns introduces perfect constraints at the contact points between them and, in a first approximation[2], these constraints are internal pivots which do not interrupt continuity of single yarns, ii) the actions which are deforming one unit cell are transmitted to closer cells via these internal pivots. Therefore, jumps in elongation and in shear deformation are not allowed as it can be seen from microscopic balance considerations. More detailed models considering friction between yarns can be obtained by following e.g. the methods used in [58]

We postpone to further investigations the quantitative analysis needed to identify the macroscopic constitutive parameters which we are going to introduce in terms of the microscopic properties of yarns. Suitable multi-scale methods as the one introduced in [59] may be generalized to be applied to the present case. Moreover, the description of the considered system at the microscopic scale may take advantage of some of the results proposed in [5, 41, 83, 70, 71, 72, 73, 74]. Indeed, we content ourselves here with the introduction of three phenomenological parameters controlling the thickness of the shear and elongation boundary layers and the value of the introduced deformation gradients.

The micromorphic hyperelastic model which we propose in this paper is based on a phenomenological approach: the addition of the micromorphic terms in the strain energy density as specified in Eq. (6) allows us to describe the existence of some regions inside the material in which high gradients of deformation occur (see also [1, 87] for the use of gradient theories to model strain localization). The onset of such boundary layers is completely accounted for by the proposed generalized hyperelastic model and will be illustrated by numerical simulations which will be subsequently compared with experimental results.

At this point, we can finally introduce the constitutive form of the micromorphic strain energy densities which will be used to describe the onset of some boundary layers which are actually observed in experimental tests on the described thin specimens of fibrous composite reinforcements. In particular, we assume that the micromorphic term appearing in Eq.(6) takes the particular form

$$W_{II}(\boldsymbol{\kappa}) = \frac{1}{2}\,\alpha_1\,\left(m_i^1\,\kappa_{ijk}\,m_j^2\right)\left(m_p^1\,\kappa_{pqk}\,m_q^2\right) + \\ +\frac{1}{2}\,\alpha_2\,\left(m_i^1\,\kappa_{ijk}\,m_j^1\right)\left(m_p^1\,\kappa_{pqk}\,m_q^1\right) + \frac{1}{2}\,\alpha_3\,\left(m_i^2\,\kappa_{ijk}\,m_j^2\right)\left(m_p^2\,\kappa_{pqk}\,m_q^2\right) \tag{12}$$

where we denoted by m_i^1 and m_j^2 the components of the vectors $\mathbf{m}_1$ and $\mathbf{m}_2$ respectively. We can then rewrite the action functional defined in (2) as

$$\mathcal{A} = \int_{B_L} \left(W_{\mathrm{I}}(\boldsymbol{\varepsilon}) + W_{II}(\boldsymbol{\kappa}) + \sum_{\alpha=1}^{3} \lambda_\alpha\, f_\alpha(\boldsymbol{\gamma}) \right),$$

where we set $n = 3$ for the number of introduced constraints which we now suppose to depend only on the relative deformation $\boldsymbol{\gamma}$. With the considered expressions of the strain energy densities $W_{\mathrm{I}}(\boldsymbol{\varepsilon})$ and $W_{II}(\boldsymbol{\kappa})$ and with the considered constraints, one can recover the particularization of the power

[2]When yarns experience a relative displacement of the contact points the macroscopic modeling may become very difficult to be obtained from microscopic considerations: an eventual attempt should be based on the methods used in [74, 75].

of internal forces given in (3) which reads

$$\mathcal{P}^{int} = \delta\mathcal{A} = \int_{B_L} \left(\left(\frac{\partial W_{\rm I}}{\partial \varepsilon_{ij}} + \sum_{\alpha=1}^{3} \lambda_\alpha \frac{\partial f_\alpha}{\partial \gamma_{hk}} \frac{\partial \gamma_{hk}}{\partial \varepsilon_{ij}} \right) \delta\varepsilon_{ij} \right)$$

$$+ \int_{B_L} \left(\sum_{\alpha=1}^{3} \lambda_\alpha \frac{\partial f_\alpha}{\partial \gamma_{hk}} \frac{\partial \gamma_{hk}}{\partial \psi_{ij}} \, \delta\psi_{ij} + \frac{\partial W_{II}}{\partial \kappa_{ijk}} \, \delta\kappa_{ijk} + \sum_{\alpha=1}^{3} f_\alpha \delta\lambda_\alpha. \right)$$

We now choose the following particular form for the constraints $f_\alpha(\boldsymbol{\gamma})$

$$f_1(\boldsymbol{\gamma}) = \mathbf{m}_1 \cdot \left(\boldsymbol{\gamma} + \frac{\mathbf{I}}{2} \right) \cdot \mathbf{m}_2, \quad f_2(\boldsymbol{\gamma}) = \mathbf{m}_1 \cdot \left(\boldsymbol{\gamma} + \frac{\mathbf{I}}{2} \right) \cdot \mathbf{m}_1, \quad f_3(\boldsymbol{\gamma}) = \mathbf{m}_2 \cdot \left(\boldsymbol{\gamma} + \frac{\mathbf{I}}{2} \right) \cdot \mathbf{m}_2.$$

In other words, recalling the definition of $\boldsymbol{\gamma}$ given in (1), we are imposing that particular projections of the micro-deformation tensor $\boldsymbol{\psi}$ on directions $\mathbf{m}_1$ and $\mathbf{m}_2$ actually tend to angle variations between the directions $\mathbf{m}_1$ and $\mathbf{m}_2$ and to macroscopic stretches in these two privileged directions. Other possible types of constraints could be included in the proposed micromorphic model which, for example, impose inextensibility of yarns so giving rise to so-called micropolar continua (see e.g. [29, 64, 28, 4, 27]). This is not the case here, since we suppose that the yarns are very stiff in elongation, but still deformable. More particularly and as it will be better seen in the following, f_1 imposes constraints on the variation of shear angle, while f_2 and f_3 impose constraints on the elongations in the two preferred directions $\mathbf{m}_1$ and $\mathbf{m}_2$. Recalling definition (1) for $\boldsymbol{\gamma}$, and that the vectors $\mathbf{m}_1$ and $\mathbf{m}_2$ are constant vectors, it is possible to verify that the power of internal forces can be finally written as

$$\mathcal{P}^{int} = \int_{B_L} \left(\frac{\partial W_{\rm I}}{\partial \varepsilon_{ij}} + \lambda_1 \, m_i^1 \, m_j^2 + \lambda_2 \, m_i^1 \, m_j^1 + \lambda_3 \, m_i^2 \, m_j^2 \right) \delta\varepsilon_{ij}$$

$$- \int_{B_L} \left(\lambda_1 m_i^1 \, m_j^2 + \lambda_2 \, m_i^1 \, m_j^1 + \lambda_3 \, m_i^2 \, m_j^2 \right) \delta\psi_{ij} \tag{13}$$

$$+ \int_{B_L} \left(\frac{\partial W_{II}}{\partial \kappa_{ijk}} \, \delta\kappa_{ijk} + \sum_{\alpha=1}^{3} f_\alpha \delta\lambda_\alpha \right).$$

It can be checked that, imposing the principle of virtual powers $\mathcal{P}^{int} = \mathcal{P}^{ext}$, where $\mathcal{P}^{int}$ and $\mathcal{P}^{ext}$ are respectively given by equations (13) and (4), and considering arbitrary variations $\delta\lambda_i$ one explicitly gets the constraints

$$f_1(\boldsymbol{\gamma}) = 0, \qquad f_2(\boldsymbol{\gamma}) = 0, \qquad f_3(\boldsymbol{\gamma}) = 0.$$

We explicitly remark that, recalling definitions (1), the constraints $f_\alpha = 0$ actually relates the micro-deformation to the macroscopic deformation as follows

$$\begin{aligned}
f_1(\boldsymbol{\gamma}) &= \mathbf{m}_1 \cdot \left(\boldsymbol{\gamma} + \frac{\mathbf{I}}{2} \right) \cdot \mathbf{m}_2 = \frac{1}{2} \, \mathbf{m}_1 \cdot (\mathbf{C} - 2\,\boldsymbol{\psi}) \cdot \mathbf{m}_2 = \frac{1}{2} \left(i_8 - \psi^1 \right) = 0, \\
f_2(\boldsymbol{\gamma}) &= \mathbf{m}_1 \cdot \left(\boldsymbol{\gamma} + \frac{\mathbf{I}}{2} \right) \cdot \mathbf{m}_1 = \frac{1}{2} \, \mathbf{m}_1 \cdot (\mathbf{C} - 2\,\boldsymbol{\psi}) \cdot \mathbf{m}_1 = \frac{1}{2} \left(i_4 - \psi^2 \right) = 0, \\
f_3(\boldsymbol{\gamma}) &= \frac{1}{2} \, \mathbf{m}_2 \cdot \left(\boldsymbol{\gamma} + \frac{\mathbf{I}}{2} \right) \cdot \mathbf{m}_2 = \frac{1}{2} \, \mathbf{m}_2 \cdot (\mathbf{C} - 2\,\boldsymbol{\psi}) \cdot \mathbf{m}_2 = \frac{1}{2} \left(i_6 - \psi^3 \right) = 0
\end{aligned} \tag{14}$$

where we set $\psi^1 := 2\,\mathbf{m}_1 \cdot \boldsymbol{\psi} \cdot \mathbf{m}_2$, $\psi^2 := 2\,\mathbf{m}_1 \cdot \boldsymbol{\psi} \cdot \mathbf{m}_1$, $\psi^3 := 2\,\mathbf{m}_2 \cdot \boldsymbol{\psi} \cdot \mathbf{m}_2$. If we now consider the constitutive expression for W_{II} given in Eq. (12), recalling that $\mathbf{m}_1$ and $\mathbf{m}_2$ are constant vectors and

that $\kappa_{ijk} = \psi_{ij,k}$, equation (13) reduces to

$$\mathcal{P}^{int} = \int_{B_L} \left(\frac{\partial W_{\mathrm{I}}}{\partial \varepsilon_{ij}} + \lambda_1 \, m_i^1 \, m_j^2 + \lambda_2 \, m_i^1 \, m_j^1 + \lambda_3 \, m_i^2 \, m_j^2 \right) \delta\varepsilon_{ij}$$

$$- \int_{B_L} \left(\lambda_1 \, m_i^1 \, m_j^2 + \lambda_2 \, m_i^1 \, m_j^1 + \lambda_3 \, m_i^2 \, m_j^2 \right) \delta\psi_{ij}$$

$$+ \int_{B_L} \left(\frac{\alpha_1}{2} \, m_i^1 \, m_j^2 \psi_{,k}^1 + \frac{\alpha_2}{2} \, m_i^1 \, m_j^1 \psi_{,k}^2 + \frac{\alpha_3}{2} \, m_i^2 \, m_j^2 \psi_{,k}^3 \right) \delta\psi_{ij,k} \, ,$$

together with the constraints $\psi^1 = i_8$, $\psi^2 = i_4$, $\psi^3 = i_6$. Recalling that $\mathbf{m}_1$ and $\mathbf{m}_2$ are constant vectors, we can write

$$m_i^1 \, m_j^2 \, \delta\psi_{ij} = \delta(m_i^1 \, m_j^2 \, \psi_{ij}) = \frac{1}{2} \, \delta\psi^1,$$

$$m_i^1 \, m_j^2 \, \delta\psi_{ij,k} = \delta \left(m_i^1 \, m_j^2 \, \psi_{ij,k} \right) = \delta \left(m_i^1 \, m_j^2 \, \psi_{ij} \right)_{,k} = \frac{1}{2} \delta(\psi_{,k}^1),$$

and analogously

$$m_i^1 \, m_j^1 \, \delta\psi_{ij} = \frac{1}{2} \, \delta\psi^2, \quad m_i^2 \, m_j^2 \, \delta\psi_{ij} = \frac{1}{2} \, \delta\psi^3$$

$$m_i^1 \, m_j^1 \, \delta\psi_{ij,k} = \frac{1}{2} \delta(\psi_{,k}^2), \quad m_i^2 \, m_j^2 \, \delta\psi_{ij,k} = \frac{1}{2} \delta(\psi_{,k}^3)$$

so that the power of internal forces, written in terms of the strain tensor $\mathbf{C}$, finally simplifies into

$$\mathcal{P}^{int} = \int_{B_L} \left(\frac{\partial W_{\mathrm{I}}}{\partial C_{ij}} + \tilde{\lambda}_1 \, m_i^1 \, m_j^2 + \tilde{\lambda}_2 \, m_i^1 \, m_j^1 + \tilde{\lambda}_3 \, m_i^2 \, m_j^2 \right) \delta C_{ij} \tag{15}$$

$$- \int_{B_L} \sum_{i=1}^{3} \tilde{\lambda}_i \, \delta\psi^i + \int_{B_L} \sum_{i=1}^{3} \tilde{\alpha}_i \, \psi_{,k}^i \, \delta(\psi_{,k}^i),$$

where we set $\tilde{\lambda}_i := \lambda/2$ and $\tilde{\alpha}_i := \alpha/4$. As for the power of external forces given in Eq. (4), we neglect body actions setting $b_i^{ext} = 0$ and $\Phi_{ij}^{ext} = 0$, and we also set $T_{ij}^{ext} = 2\tilde{\beta}_1^{ext} \, m_i^1 \, m_j^2 + 2\tilde{\beta}_2^{ext} \, m_i^1 \, m_j^1 + 2\tilde{\beta}_3^{ext} \, m_i^2 \, m_j^2$, so that the principle of virtual powers $\mathcal{P}^{int} = \mathcal{P}^{ext}$ finally implies

$$\int_{B_L} \left(\frac{\partial W_{\mathrm{I}}}{\partial C_{ij}} + \tilde{\lambda}_1 \, m_i^1 \, m_j^2 + \tilde{\lambda}_2 \, m_i^1 \, m_j^1 + \tilde{\lambda}_3 \, m_i^2 \, m_j^2 \right) \delta C_{ij}, \tag{16}$$

$$- \int_{B_L} \sum_{i=1}^{3} \tilde{\lambda}_i \delta\psi^i + \int_{B_L} \sum_{i=1}^{3} \tilde{\alpha}_i \, \psi_{,k}^i \, \delta(\psi_{,k}^i) = \int_{\partial B_L} t_i^{ext} \delta u_i + \int_{\partial B_L} \sum_{i=1}^{3} \tilde{\beta}_i^{ext} \, \delta\psi^i,$$

together with the constraints $\psi^1 = i_8$, $\psi^2 = i_4$ and $\psi^3 = i_6$. We remark that the considered expression for the external double forces, actually allows to consider external actions which expend power on shear angle variations and on fiber elongation. In this way, one has the possibility to act on the boundary of considered material assigning force or displacement, shear double force or shear angle variation and also elongation double force or fiber elongation.

We finally want to explicitly remark that Eq. (16) actually represents a very particular case of second gradient theory. In fact, using the constraints $\psi^1 = i_8$, $\psi^2 = i_4$ and $\psi^3 = i_6$ one gets

$$\delta\psi^1 = \delta i_8 = m_i^1\, m_j^2\, \delta C_{ij}, \quad \delta\psi^2 = \delta i_4 = m_i^1\, m_j^1\, \delta C_{ij}, \quad \delta\psi^3 = \delta i_6 = m_i^2\, m_j^2\, \delta C_{ij},$$

$$\delta(\psi^1_{,k}) = \delta(i_8)_{,k} = m_i^1\, m_j^2\, \delta C_{ij,k},\ \delta(\psi^2_{,k}) = \delta(i_4)_{,k} = m_i^1\, m_j^1\, \delta C_{ij,k},\ \delta(\psi^3_{,k}) = \delta(i_6)_{,k} = m_i^2\, m_j^2\, \delta C_{ij,k}$$

so that Eq. (16) is also equivalent to

$$\int_{B_L} \left[\frac{\partial W_{\rm I}}{\partial C_{ij}}\, \delta C_{ij} + \left(\tilde{\alpha}_1 \left(m_p^1\, m_q^2\, C_{pq,k}\right) m_i^1\, m_j^2 + \tilde{\alpha}_2 \left(m_p^1\, m_q^1\, C_{pq,k}\right) m_i^1\, m_j^1 + \tilde{\alpha}_3 \left(m_p^2\, m_q^2\, C_{pq,k}\right) m_i^2\, m_j^2\right) \delta C_{ij,k} \right]$$

$$= \int_{\partial B_L} t_i^{ext} \delta u_i + \int_{\partial B_L} \left(\tilde{\beta}_1^{ext}\, m_i^1\, m_j^2 + \tilde{\beta}_2^{ext}\, m_i^1\, m_j^1 + \tilde{\beta}_3^{ext}\, m_i^2\, m_j^2\right) \delta C_{ij} \tag{17}$$

We have hence explicitly recovered a special second gradient theory starting from the proposed constrained micromorphic model. Nevertheless, in our numerical simulations, instead of using the second gradient weak form (17), we use the constrained micromorphic one (16). The advantage of using the micromorphic approach instead of directly using a second gradient theory is that the boundary conditions which can be imposed are, in the present case, more easily understandable from a physical point of view. In particular, we remark that, for example, under the constraints $\psi^1 = i_8$, the fact of imposing $\psi^1 = 0$ on the boundary means that we are imposing zero variation of the angle between the fibers. Analogously, under the constraints $\psi^2 = i_4$ and $\psi^3 = i_6$, imposing $\psi^2 = 1$ and $\psi^3 = 1$ is equivalent to prevent elongation in the preferred directions $\mathbf{m}_1$ and $\mathbf{m}_2$. We therefore end up with a model in which it is possible to impose, at the boundary of considered system, both the displacement field and the deformation fields measuring variation of the angle between fibers and elongations along the two preferred directions. The generalized theory proposed in this paper becomes essential for describing deformation patterns in which high gradients of deformation occur in relatively narrow regions of the material. This is the case for the deformation patterns which will be described in the next section.

4. Phenomenology of the bias extension test

The bias extension test is a mechanical test which is very well known in the field of composite materials manufacturing (see e.g. [11, 40, 63]). It is widely used to characterize the mechanical behavior of woven-fabric fibrous composite preforms undergoing large shear deformations. Such fibrous materials have attracted significant attention from both industry and academia, due to their high specific strength and stiffness as well as their excellent formability characteristics. These materials are widely being used in the aerospace industry since they provide a suitable compromise between high mechanical performances, light weight and easy shaping. The bias extension test is performed on rectangular samples of woven composite reinforcements, with the height (in the loading direction) relatively greater (at least twice) than the width, and the yarns initially oriented at $\pm$ 45-degrees with respect to the loading direction. The specimen is clamped at two ends, one of which is maintained fixed and the second one is displaced of a given amount. The relative displacement of the two ends of the specimen provokes angle variations between the warp and weft: the creation of three different regions A, B and C, in which the shear angle between fibers remains almost constant after deformation, can be detected (see Fig. 3). In particular, the fibers in regions C remain undeformed, i.e. the angle between fibers remains at 45° also after deformation. On the other hand, the angle between fibers becomes much smaller than 45° in regions A and B, but it keeps almost constant in each of them. The main characteristics of the bias extension test are summarized in Fig. 3 in which both the undeformed and deformed shapes of the considered specimen are depicted. The specimen is clamped at its two ends using specific tools which impose the following boundary conditions:

- vanishing displacement at the bottom of the specimen,
- assigned displacement at the top of the specimen

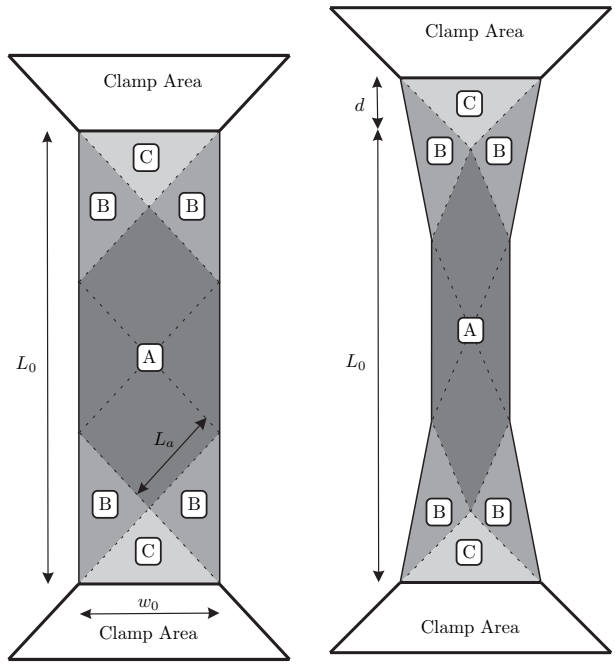

FIGURE 3. Simplified description of the deformation pattern in the bias extension test.

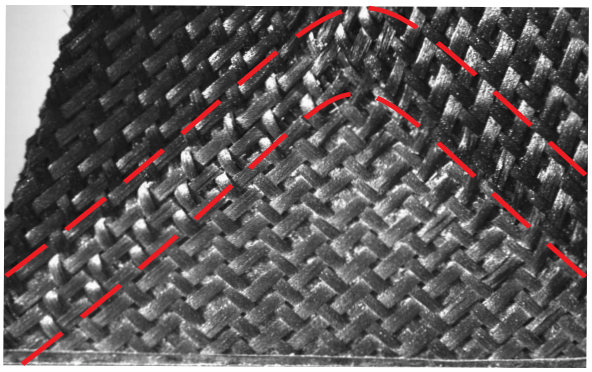

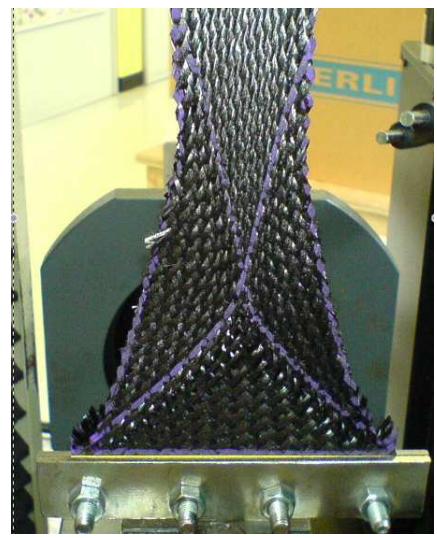

FIGURE 4. Boundary layers between two regions at constant shear (left) and curvature of the free boundary (right).

- fixed angle between the fibers (45°) at both the top and the bottom of the specimen.
- vanishing elongation of the fibers at both the top and the bottom of the specimen.

It is clear that the third type of boundary condition which imposes that the angle between fibers cannot vary during deformation of the specimen is a boundary condition which, at the level of a macro model, imposes deformation and not displacement. The same is for the fourth type of boundary conditions blocking elongation of fibers. Boundary conditions of this type cannot be accounted for in a first

gradient theory, while they can be naturally included in a second gradient one, as duly explained in the previous section.

Moreover, the deformation scheme described in Fig. 3 does not take into account some specificity of the deformations which are actually observed during a bias extension test. In particular, the following two experimental evidences are not included in the scheme presented in the quoted figure:

- the presence of transition layers between two adjacent zones with constant shear deformation
- the more or less pronounced curvature of the free boundaries of the specimen.

Indeed, both these evidences can be observed in almost any bias extension test on woven composite preforms, as it is shown in Fig. 4.

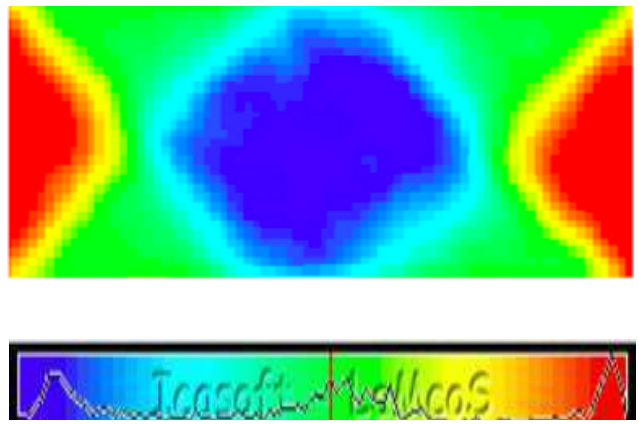

FIGURE 5. Contour of shear angle in a bias-extension test obtained from the optical measurement software Icasoft (INSA-Lyon).

A set of bias tests run on specimens under identical circumstances have produced some suggestive results which were gathered in a picture of [11] which we reproduce here in Fig. 5. In this figure the contour of the shear angle variation between yarns is depicted as the result of some optical measurements conducted at INSA-Lyon. Unfortunately, the yarns constituting the considered reinforcements have a very high extensional rigidity and, as a consequence, the tickness of the corresponding elongation boundary layers is relatively smaller. Hence, in order to obtain similar results for the elongation boundary layers, suitably targeted measurement campaigns should be conceived.

The principle of virtual powers for constrained micromorphic media formulated in Eq. (16) allows for the description of the onset of thin boundary layers in which high gradients of shear deformation occur and which allow for a gradual transition from one value of the shear angle to the other one. The onset of these boundary layers cannot be accounted for by a first gradient theory, while it can be described by adding a dependence of the energy density on gradients of the shear deformation. Curvature effects will be also pointed out in the results obtained in the performed numerical simulations and which will be shown in the next section.

5. Numerical simulations

We now propose to apply the introduced second gradient model to perform numerical simulations of the bias extension test which take into account the onset of shear boundary layers. We consider a rectangular specimen of 100 mm of width of and 300 mm of height in the undeformed configuration. The fibers are at $\pm 45^\circ$ with respect to the direction of the height of the specimen in the undeformed configuration. To perform the numerical simulations we choose a fixed orthonormal basis such that,

TABLE 1. Constitutive first gradient coefficients used in the numerical simulations.

K^0_{elong}	K^1_{elong}	I^0_{elong}	K^{12}_{shear}	K^{21}_{shear}	p	W^0_{shear}	I^0_{shear}
[MPa]	[MPa]	[−]	[MPa]	[MPa]		[MPa]	[−]
37.85	816.33	1.45×10^{-2}	0.07575	1.69×10^{-4}	3.69	-1.69×10^{-4}	4.20×10^{-3}

the components of the two structural vectors introduced before are $\mathbf{m}_1 = \left(\sqrt{2}/2, \sqrt{2}/2, 0\right)^T$ and $\mathbf{m}_2 = \left(\sqrt{2}/2, -\sqrt{2}/2, 0\right)^T$ and we impose at the top of the specimen a vertical displacement $d = 55mm$. Clearly, also the deformation tensor $\mathbf{C}$ and all its introduced invariants can be accordingly written in the chosen basis. We summarize in Tab. 1 the values of the first gradient constitutive parameters appearing in the orthotropic hyperelastic potential (11) which are used to perform the numerical simulations presented in this section. These values have been proposed in [14] as the result of specific measurement campaigns.

5.1. First gradient limit solution

As discussed in detail by [38, 39], first gradient energies, in which the physical phenomena governing the onset of boundary layers are neglected, actually produce mesh-dependent numerical simulations. To remedy to this circumstance, [82] suggested some techniques whose numerical counterpart has been developed in [38, 39] for considered case: following the ideas there exposed we could get numerical simulations in which boundary layers reduce to lines and deformation measures are subjected to jumps. We show the result of one of these numerical simulations in Fig. 6. This picture represents the

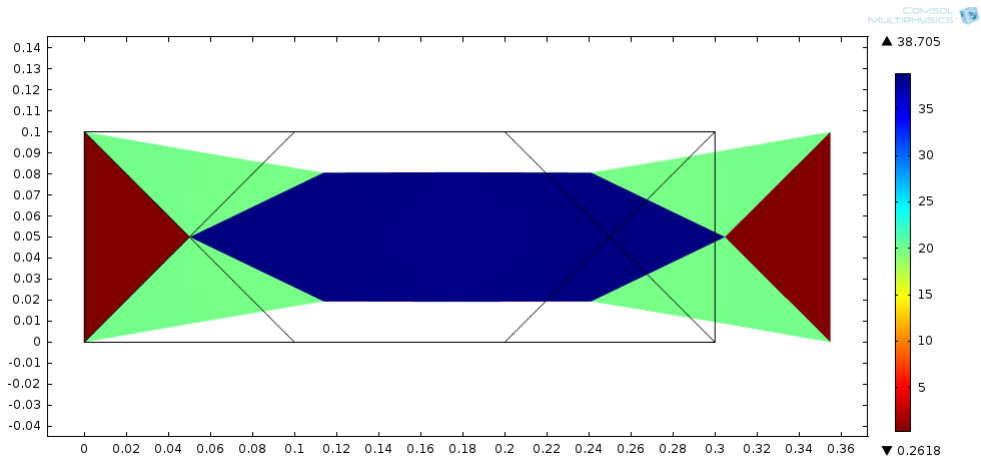

FIGURE 6. Shear angle variation ϕ for an imposed displacement $d = 55\,mm$ obtained with the first gradient theory. The lateral bar indicates the values of ϕ in degrees.

shear deformation field which is the correct limit to which regularized models must converge when higher gradient parameters tend to zero. In particular, figure 6 shows the shear angle variation ϕ which is obtained as solution of the first gradient equilibrium problem resulting from (16) by setting $\tilde{\alpha}_1 = \tilde{\alpha}_2 = \tilde{\alpha}_3 = 0$ and $\tilde{\beta}_1^{ext} = \tilde{\beta}_2^{ext} = \tilde{\beta}_3^{ext} = 0$. The boundary conditions which have been used to solve the first gradient equilibrium problem are

- Vanishing displacement on the left surface: $\delta u_i = 0,\ i = \{1, 2\}$,
- Assigned displacement on the right surface: $\delta u_1 = 55\,mm,\ \delta u_2 = 0$,
- Unloaded lateral (top and bottom) surfaces (i.e. $t_i^{ext} = 0,\ i = \{1, 2\}$).

As it can be seen, the three zones A, B and C defined in Fig. 3 can be identified in the solution shown in Fig. 6: the red zones (corresponding to zones C) are such that no angle variation occurs with respect to the reference configuration ($\phi = 0$). On the other hand, the green and the blue zones respectively correspond to regions B and A and are such that two different constant angle variations ($\phi_B \approx \phi_A/2 \neq 0$) with respect to the reference configuration occur. The first gradient solution is such that a sharp interface between each pair of the three shear regions can be observed.

5.2. Second gradient solution and the onset of boundary layers

For what concerns the solution which we have obtained by means of the introduced second gradient model, we start by heuristically choose the values of the second gradient parameters by using an inverse method based on physical observations. However, further investigations are needed to establish a theoretical relationship between the microscopic structure of considered reinforcements and the macroscopic parameters here introduced: it is indeed well known (see e.g. [12, 16, 17, 34]) that the second gradient parameters are intrinsically related to a characteristic length L_c which is, in turn, associated to the micro-structural properties of considered materials. It is also known that many identification methods have been introduced to relate the macroscopic second gradient parameter to the microscopic properties of the considered medium. Some of these methods are presented in [3, 81]. Calling L_c the measured thickness of the shear boundary layer highlighted in Fig. 4, we tune the value of the second gradient parameters $\tilde{\alpha}_i,\ i = \{1, 2, 3\}$ in our numerical simulations until we obtain a boundary layer having the same thickness L_c. In particular, for a characteristic length $L_c \approx 2\ cm$, we obtain, by inverse approach, the following values of the shear and elongation second gradient parameters respectively

$$\tilde{\alpha}_1 = 3 \times 10^{-5} MPa\, m^2, \quad \tilde{\alpha}_2 = \tilde{\alpha}_3 = 9 \times 10^{-3}\, MPa\, m^2.$$

The second gradient solution for the shear angle variation ϕ, obtained for the aforementioned values of the second gradient parameters, is shown in Fig. 7. For obtaining this solution, Eq. (16) was solved with the following additional boundary conditions

- Zero angle variation at the clamped ends of the specimen: $\psi^1 = i_8 = 0$,
- Zero elongation of the fibers at the clamped ends of the specimen: $\psi^2 = i_4 = 1$, $\psi^3 = i_6 = 1$.
- Boundaries on the lateral (top and bottom) surfaces free from micromorphic loads: $\tilde{\beta}_i^{ext} = 0,\ i = \{1, 2\}$.

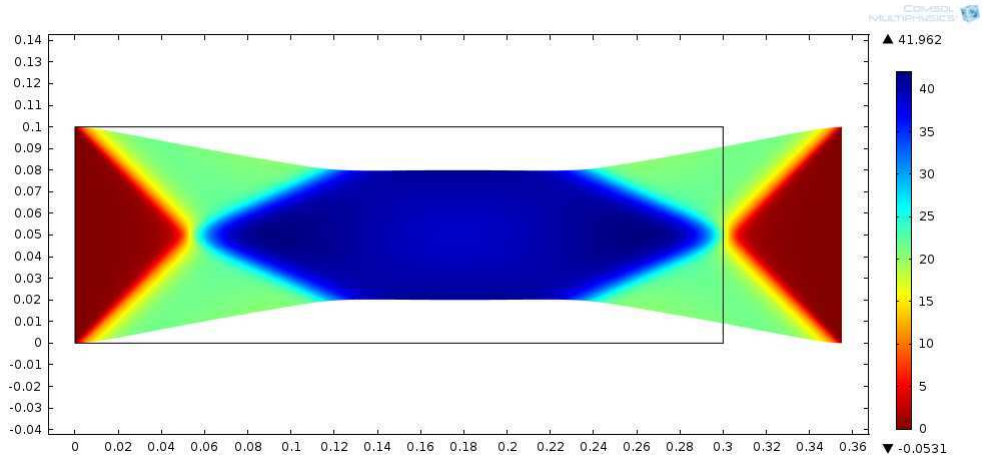

FIGURE 7. Shear angle variation ϕ for an imposed displacement $d = 55\,mm$ obtained with the proposed second gradient theory. The lateral bar indicates the values of ϕ in degrees

It can be noticed that in the second gradient solution shown in Fig. 7 the transition zones between different shear regions are regularized and shear boundary layers can be clearly observed, as well as a curvature of the free boundaries on the two free sides. It can be immediately remarked how the solution shown in Fig. 7 is, at least qualitatively, very close to the experimental picture shown in Fig.5.

We show in Fig. 8 the first and second gradient solutions for the shear angle variation along the sections I and II. It can be clearly seen that, along section I, the first gradient solution (dashed line)

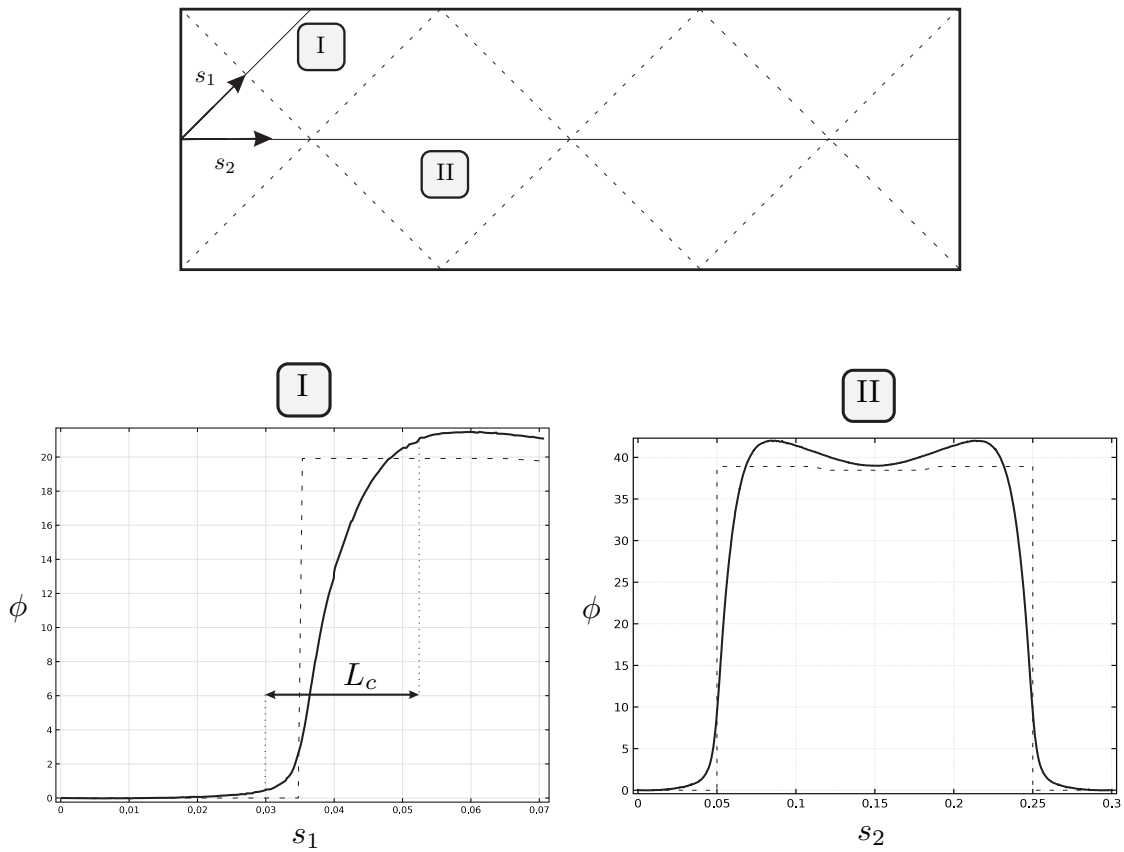

FIGURE 8. Definition of the sections I and II (top) and shear angle variation ϕ for the two sections I and II both for first gradient (dashed line) and second gradient (continuous line).

produces a sharp variation of the shear angle across the two regions C and B. On the other hand, the second gradient solution (continuous line) clearly regularizes the transition between the zone at zero variation of the shear angle and the adjacent zone. The same arrives in section II, which spans on the whole specimen, in which the transition zones are clearly regularized by the second gradient solution.

In Fig. (9) we show the effect of the variation of the shear second gradient parameter $\tilde{\alpha}_1$ on the solution for the shear angle variation ϕ along the sections I and II respectively. It can be seen that the effect of increasing the shear second gradient parameter actually lower the value of the shear angle variation so producing more regular transitions from the two regions at different constant shear. This clearly results in an increasing of the characteristic size of the shear boundary layer. It can be also noticed that the value of ϕ increases with $\tilde{\alpha}_1$ in the center of the specimen. We can conclude

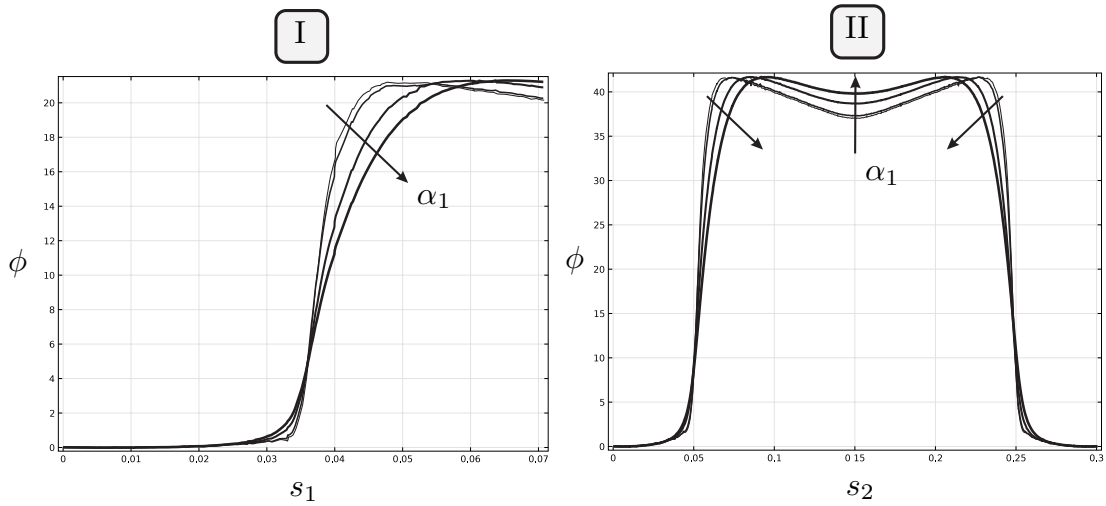

FIGURE 9. Parametric study on the shear second gradient parameter $\tilde{\alpha}_1 \in [7 \times 10^{-6}, 6 \times 10^{-5}]$ $MPa\,m^2$, taking fixed $\tilde{\alpha}_2 = \tilde{\alpha}_3 = 9 \times 10^{-3}$ $MPa\,m^2$.

that the choice of the shear second gradient parameter $\tilde{\alpha}_1$ is directly related to the fact of fixing the thickness of the shear boundary layer. This parameter can be hence easily tuned on the basis of experimental evidences. In the presented numerical simulations, we tuned the shear second gradient parameter $\tilde{\alpha}_1$ in order to have a boundary layer of thickness $L_c \approx 2\ cm$, so obtaining the quoted value $\tilde{\alpha}_1 = 3 \times 10^{-5} MPa\,m^2$.

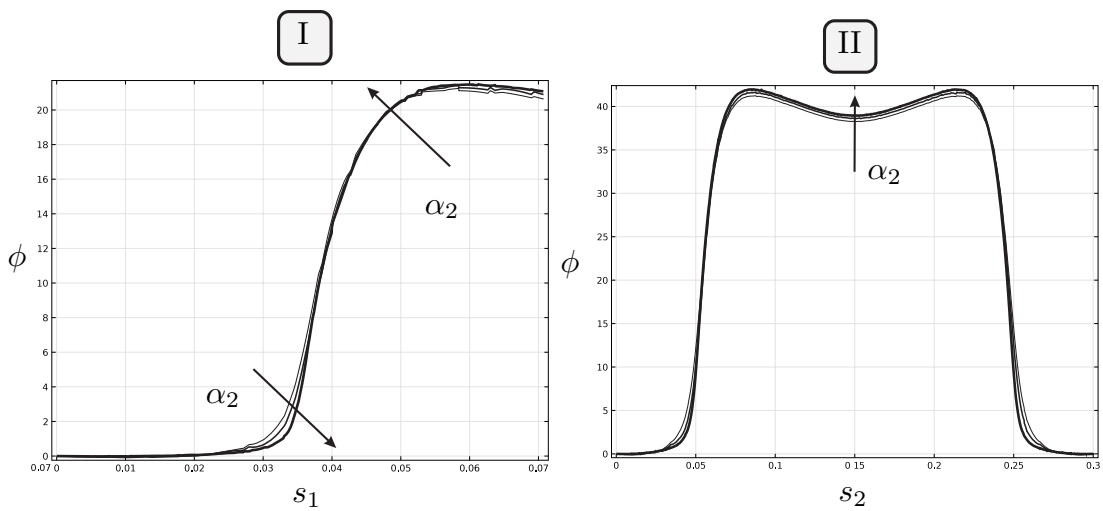

FIGURE 10. Parametric study on the elongation second gradient parameter $\tilde{\alpha}_2 = \tilde{\alpha}_3 \in [3 \times 10^{-3}, 9 \times 10^{-3}]$ $MPa\,m^2$, taking fixed $\tilde{\alpha}_1 = 3 \times 10^{-5}$ $MPa\,m^2$.

As for the choice of the second gradient elongation parameters, the identification procedure is less direct than that one used for identifying the shear parameter $\tilde{\alpha}_1$. First of all, due to symmetry of material properties in the directions of weft and warp, we set *a priori* that $\tilde{\alpha}_2 = \tilde{\alpha}_3$. Unfortunately, due to the very high tensile stiffness of the yarns, experimental measurements of elongation boundary layers in the fiber directions are not available, as it was instead the case for shear boundary layers

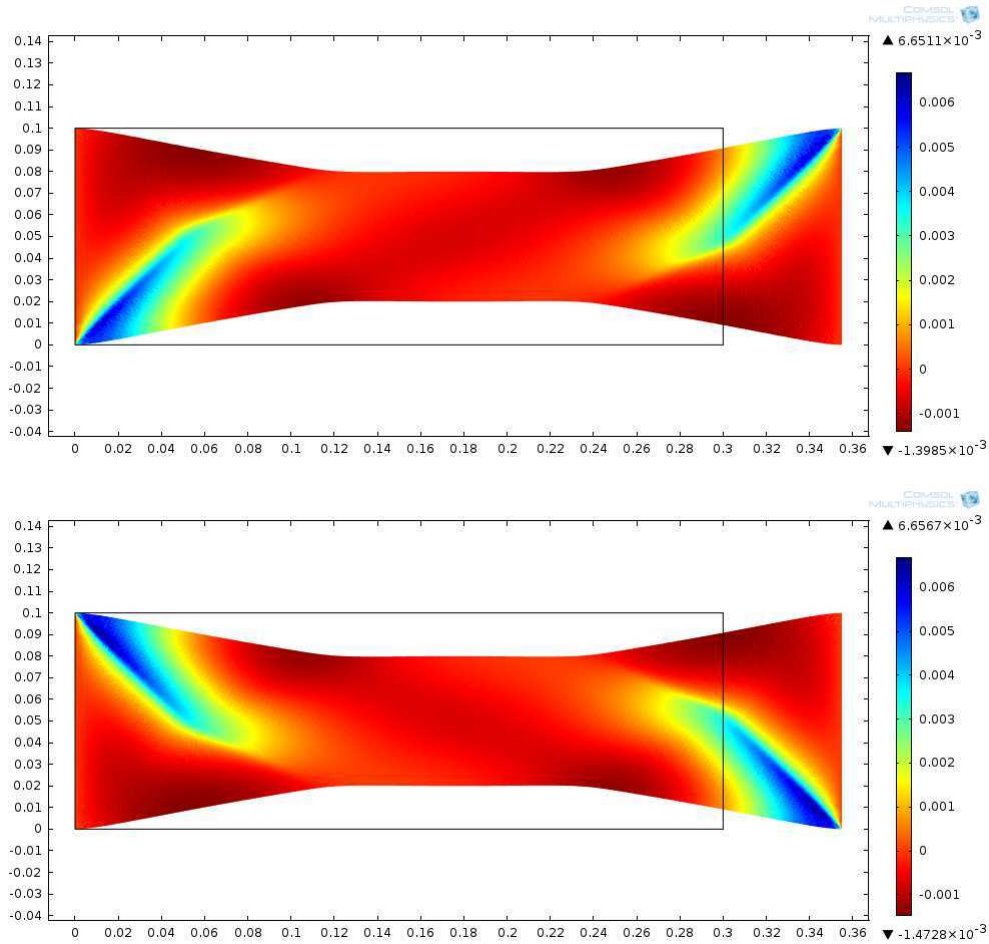

FIGURE 11. Elongations in the direction + 45° (top figure) and -45° (bottom figure).

(see Fig. 5). The precise tuning procedure which allows us to fit the second gradient elongation parameters to experimental measures of elongation boundary layers is henceforth not possible at this stage. Therefore, the value of the parameters $\tilde{\alpha}_2$ and $\tilde{\alpha}_3$ was tuned after performing the parametric study shown in Fig. 10 in which the effect of the variation of the second gradient elongation parameter on the value of the shear angle is shown. It can be remarked from this picture that increasing the value of the second gradient elongation parameter results in an overall increase of the shear angle variation ϕ. The value of $\tilde{\alpha}_2$ which gives, in the center of the specimen, the same value of ϕ obtained for the limit first gradient solution shown in Fig. 6 was chosen, so resulting in the value $\tilde{\alpha}_2 = 9 \times 10^{-3} MPa\, m^2$. We obtained, in the performed numerical simulations, an elongation field which is everywhere very small: the maximum value of elongation is of the order of 10^{-3}. We show in figures 11 the elongation boundary layers (each corresponding to the elongation in one of the two preferred directions of the fibers) obtained in the performed numerical simulations. In order to precisely reveal the nature of these elongation boundary layers suitable experimental campaigns as well as adapted microscopic models should be developed together with suitable micro-macro identification techniques.

5.3. By using first gradient models it is not possible to correctly describe the onset of boundary layers

One could wonder if it is really necessary to introduce micromorphic continuum models to carefully describe the onset of boundary layers in bias tests. In the present subsection we discuss some difficulties

which arise if one tries to use the methods discussed in section 5.1. Actually, as shown by Fig. 12, although it is indeed possible to describe the onset of some boundary layers still remaining in the framework of first gradient models, it seems very unlikely that with those methods one can catch all experimental features which are present in bias extension tests. In the numerical simulations leading to Fig. 12 one can see formation of boundary layers where high gradients of shear and elongation are concentrated even if this simulation is conducted in the framework of first gradient theory. However, the solution is qualitatively and quantitatively different from the first gradient sharp solution shown in Fig. 6 so that realistic quantitative values for shear deformations cannot be obtained from it. Moreover, if one evaluates the reaction force on the fixed clamped end in the last considered case,

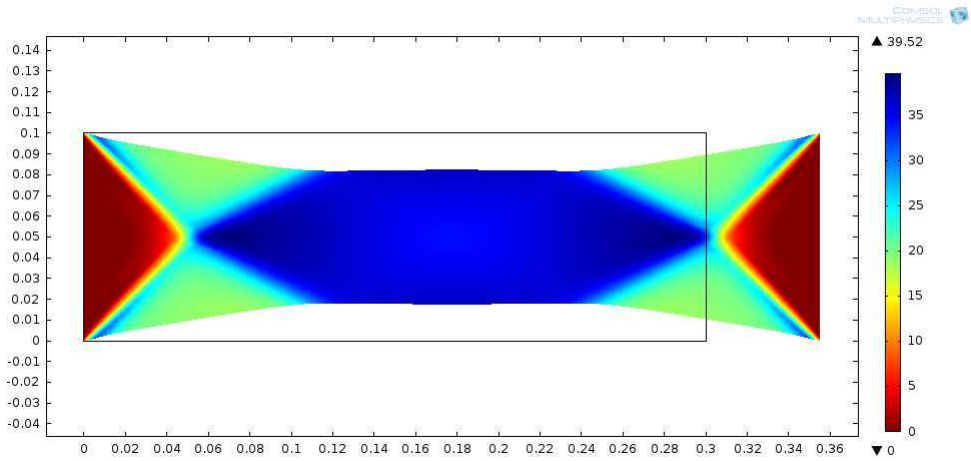

FIGURE 12. Shear angle variation ϕ for an imposed displacement $d = 55mm$ obtained with the first gradient theory and for an arbitrary mesh. The lateral bar indicates the values of ϕ in degrees

it can be checked that its value exceeds of a big amount the reaction force which is expected. More particularly, the force evaluated for the limit first gradient solution depicted in Fig. 6 is of the order of 5 N which is a sensible force for the bias extension test. On the other hand, if one evaluates the force for the case depicted in Fig. 12, this force exceeds from 10 to 100 times the 5 N obtained in the limit sharp first gradient solution, depending on the choice of the mesh. This means that the mesh dependence of the first gradient solution is even more evident when analyzing force than when analyzing deformation. Such a problem on the value of calculated force is not present when considering the second gradient solution shown in Fig. 7. This point allows us to conclude that, using first gradient models, it is not possible to correctly describe the onset of boundary layers and that the reaction forces at clamped ends are definitely overestimated as soon as one gets far from the limit first gradient solution shown in Fig. 6.

6. Conclusions

In this paper a constrained micromorphic theory is introduced which includes, as a particular case, a second gradient model. Particular orthotropic, hyperelastic, constitutive laws are introduced in order to account for the anisotropy of fibrous composite reinforcements undergoing large deformations. The obtained theoretical framework is used to model the mechanical behavior of such fibrous composite materials during the so-called bias extension test.

The first and second gradient solutions are compared showing that the proposed second gradient model is actually able to describe the onset of shear boundary layers which regularize the first gradient sharp transition between two zones at different levels of shear. Moreover, differently from what happens

for the first gradient model, the proposed second gradient theory also allows to describe the curvature of the free boundaries of the specimen.

In order to identify the values of introduced second gradient parameters we proceed by inverse approach, performing numerical simulations which correctly fits the experimental data. More particularly, we choose the values of second gradient parameters in order to fit at best the characteristic length of the shear boundary layer which is observed is bias test experiments.

Therefore, the results obtained in this paper allow us to estimate the order of magnitude of the second gradient parameters to be used for the considered fibrous materials. These results are promising and justify the need of novel experimental campaigns in order to estimates such gradient parameters for a wider class of composite preforms.

References

[1] Aifantis E.C., 1992. On the role of gradients in the localization of deformation and fracture. International Journal of Engineering Science 30:10, 1279-1299

[2] Aimène Y., Vidal-Sallé E., Hagège B., Sidoroff F., Boisse P., 2010. A hyperelastic approach for composite reinforcement large deformation analysis. J. Compos. Mater., 44:1, 5-26

[3] Alibert J.-J., Seppecher P., Dell'Isola F., 2003. Truss modular beams with deformation energy depending on higher displacement gradients. Math. Mech. Solids 8:1, 51-73

[4] Altenbach H., Eremeyev V.A., Lebedev L.P., Rendón L.A. (2010). Acceleration waves and ellipticity in thermoelastic micropolar media Archive of Applied Mechanics 80 (3), 217-227

[5] Atai, A.A., Steigmann, D.J. (1997). On the nonlinear mechanics of discrete networks Archive of Applied Mechanics, 67:5, 303-319

[6] Balzani D., Neff P., Schröder J., Holzapfel G.A., (2006). A polyconvex framework for soft biological tissues, Adjustment to experimental data. Int. J. Solids Struct., 43, 6052-6070

[7] Bleustein J.L., 1967. A note on the boundary conditions of Toupin's strain gradient-theory. Int. J. Solids Structures, 3, 1053-1057.

[8] Boehler, J.P., 1987. Introduction to the invariant formulation of anisotropic constitutive equations. In: Boehler, J.P. (Ed.), Applications of Tensor Functions in Solid Mechanics CISM Course No. 292. Springer-Verlag.

[9] Boehler JP. Lois de comportement anisotrope des milieux continus. J Méc 1978;17:153-70

[10] Boisse P., Cherouat A., Gelin J.C., Sabhi H., 1995. Experimental Study and Finite Element Simulation Of Glass Fiber Fabric Shaping Process. Polymer Composites 16:1, 83-95

[11] Cao J., Akkerman R., Boisse P., Chen J., et al., 2008. Characterization of mechanical behavior of woven fabrics: experimental methods and benchmark results. Compos. Part A: Appl. Sci. Manuf. 39, 1037-53.

[12] Casal P., 1972. La théorie du second gradient et la capillarité. C.R. Acad. Sci. Paris, Ser. A 274, 1571-1574

[13] Charmetant A., Vidal-Sallé E., Boisse P. (2011). Hyperelastic modelling for mesoscopic analyses of composite reinforcements. Composites Science and Technology, 71,1623-1631

[14] Charmetant A., Orliac J.G.,Vidal-Sallé E., Boisse P. (2012). Hyperelastic model for large deformation analyses of 3D interlock composite preforms. Composites Science and Technology, 72, 1352-1360

[15] Cosserat E., Cosserat F., 1909. Théorie de Corps déformables. Librairie Scientifique A. Hermann et fils, Paris

[16] deGennes, P.G., 1981. Some effects of long range forces on interfacial phenomena. J. Phys. Lett. 42, L377–L37

[17] dell'Isola F., Gouin H., Seppecher P., 1995. Radius and surface tension of microscopic bubbles by second gradient theory. C.R. Acad. Sci. II, Mec. 320, 211-216

[18] dell'Isola F., Rotoli G., 1995. Validity of Laplace formula and dependence of surface tension on curvature in second gradient fluids. Mechanics Research Communications, 22, 485-490

[19] dell'Isola F., Seppecher P., 1995. The relationship between edge contact forces, double force and interstitial working allowed by the principle of virtual power, C.R. Acad. Sci. II, Mec. Phys. Chim. Astron. 321, 303-308

[20] dell'Isola F., Gouin H., Rotoli G., 1996. Nucleation of Spherical shell-like interfaces by second gradient theory: numerical simulations, Eur. J. Mech. B, Fluids 15:4, 545-568

[21] dell'Isola F., Seppecher P., 1997. Edge contact forces and quasi-balanced power, Meccanica 32, 33-52

[22] dell'Isola F., Guarascio M., Hutter K., 2000. A variational approach for the deformation of a saturated porous solid. A second-gradient theory extending Terzaghi's effective stress principle. Archive of Applied Mechanics. 70, 323-337.

[23] dell'Isola F., Sciarra G., and Vidoli S., 2009. Generalized Hooke's law for isotropic second gradient materials, Proc. R. Soc. Lond. A 465, 2177–2196.

[24] dell'Isola F., Madeo A., Placidi L., 2012. Linear plane wave propagation and normal transmission and reflection at discontinuity surfaces in second gradient 3D Continua. Zeitschrift fur Angewandte Mathematik und Mechanik (ZAMM), 92:1, 52-71

[25] dell'Isola F., Seppecher P., Madeo A., 2012. How contact interactions may depend on the shape of Cauchy cuts in N-th gradient continua: approach "à la D'Alembert". ZAMP, 63:6, 1119-1141

[26] Dumont J.P., Ladeveze P., Poss M., Remond Y., 1987. Damage mechanics for 3-D composites Composite structures, 8:2, 119-141

[27] Eremeyev V. A., Lebedev L. P., Altenbach H. (2013). Foundations of micropolar mechanics. Springer, Heidelberg.

[28] Eremeyev V.A., 2005. Acceleration waves in micropolar elastic media. Doklady Physics 50:4, 204-206

[29] Eringen A. C., 2001. Microcontinuum field theories. Springer-Verlag, New York.

[30] Eringen A.C., Suhubi, E.S. 1964. Nonlinear theory of simple microelastic solids: I. Int. J. Eng. Sci., 2, 189-203.

[31] Eringen A. C., Suhubi, E. S. 1964. Nonlinear theory of simple microelastic solids: II. Int. J. Eng. Sci., 2, 389-404.

[32] Forest, S., Sievert, R. 2006. Nonlinear microstrain theories. Int. J. Solids Struct., 43, 7224-7245.

[33] Forest S. 2009. Micromorphic Approach for Gradient Elasticity, Viscoplasticity, and Damage. Journal of Engineering Mechanics, 135:3, 117-131.

[34] Forest S., Aifantis E.C., 2010. Some links between recent gradient thermo-elasto-plasticity theories and the thermomechanics of generalized continua. Int. J. Solids. Struct. 47:(25-26), 3367-3376

[35] Germain, P., 1973. La méthode des puissances virtuelles en mécanique des milieux continus. Première partie. Théorie du second gradient. J. Mécanique 12, 235-274.

[36] Germain, P., 1973. The method of virtual power in continuum mechanics. Part 2: Microstructure. SIAM J. Appl. Math. 25, 556-575

[37] Green A.E., Rivlin R.S., 1964. Multipolar continuum mechanics. Archive for Rational Mechanics and Analysis, 17: 2, 113-147

[38] Hamila N., Boisse P., 2013. Tension locking in finite-element analyses of textile composite reinforcement deformation. Comptes Rendus Mécanique, 341:6, 508-519.

[39] Hamila N., Boisse P., 2013. Locking in simulation of composite reinforcement deformations. Analysis and treatment. Composites Part A: Applied Science and Manufacturing, DOI: http://dx.doi.org/10.1016/j.compositesa.2013.06.001

[40] Harrison P., Clifford M.J., Long A.C. 2004. Shear characterisation of viscous woven textile composites: a comparison between picture frame and bias extension experiments. Composites Science and Technology, 64, 1453-1465

[41] Haseganu, E.M., Steigmann, D.J. (1996). Equilibrium analysis of finitely deformed elastic networks. Computational Mechanics, 17:6, 359-373

[42] Holzapfel, G.A., Gasser, T.C., Ogden, R.W., 2000. A new constitutive framework for arterial wall mechanics and a comparative study of material models. Journal of Elasticity 61, 1-48.

[43] Holzapfel, G.A., 2000. Nonlinear Solid Mechanics, Wiley.

[44] Itskov M., Aksel N., 2004. A class of orthotropic and transversely isotropic hyperelastic constitutive models based on a polyconvex strain energy function. Int. J. Solids Struct., 41, 3833–3848

[45] Itskov M. 2000. On the theory of fourth-order tensors and their applications in computational mechanics. Comput Methods Appl. Mech. Eng., 189:2, 419-38

[46] Lasry D., Belytschko T., 1988. Localization limiters in transient problems. Int. J. Solids Struct., 24: 6, 581-597.

[47] Lee W., Padvoiskis J., Cao J., de Luycker E., Boisse P., Morestin F., Chen J., Sherwood J., 2008. Bias-extension of woven composite fabrics. Int J Mater Form Suppl 1:895-898

[48] Luongo A. (1991). On the amplitude modulation and localization phenomena in interactive buckling problems. International Journal of Solids and Structures 27:15, 1943-1954

[49] Luongo A. (2001). Mode localization in dynamics and buckling of linear imperfect continuous structures. Nonlinear Dynamics 25:1, 133-156

[50] Luongo A., D'Egidio A. (2005). Bifurcation equations through multiple-scales analysis for a continuous model of a planar beam. Nonlinear Dynamics 41:1, 171-190

[51] Madeo A., George D., Lekszycki T., Nieremberger M., Rémond Y., 2012. A second gradient continuum model accounting for some effects of micro-structure on reconstructed bone remodelling. CRAS Mécanique, 340:8, 575-589

[52] A. Madeo, F. dell'Isola, N. Ianiro and G. Sciarra, 2008. A Variational Deduction of Second Gradient Poroelasticity II: an Application to the Consolidation Problem. Journal of Mechanics of Materials and Structures, 3:4, 607-625

[53] Madeo A., dell'Isola F., Ianiro N., SciarraG., 2008. A variational deduction of second gradient poroelasticity II: An application to the consolidation problem, J. Mech. Mater. Struct. 3:4, 607-625

[54] Madeo A., Djeran-Maigre I., Rosi G., Silvani C., 2012. The Effect of Fluid Streams in Porous Media on Acoustic Compression Wave Propagation, Transmission and Reflection. Continuum Mechanics and Thermodynamics, DOI: 007/s00161-012-0236-y

[55] Makradi A., Ahzi S., Garmestani H., Li D.S., Rémond Y., 2010. Statistical continuum theory for the effective conductivity of fiber filled polymer composites: Effect of orientation distribution and aspect ratio A Mikdam. Composites Science and Technology 70 :3, 510-517

[56] Mikdam A., Makradi A., Ahzi S., Garmestani H., Li D.S., Rémond Y., 2009. Effective conductivity in isotropic heterogeneous media using a strong-contrast statistical continuum theory. Journal of the Mechanics and Physics of Solids 57:1, 76-86

[57] Mindlin R.D. , 1964. Micro-structure in linear elasticity. Archs ration. Mech. Analysis 51-78

[58] Nadler, B., Steigmann, D.J. (2003). A model for frictional slip in woven fabrics. Comptes Rendus - Mecanique, 331 (12), pp. 797-804

[59] Nadler, B., Papadopoulos, P., Steigmann, D.J. (2006). Multiscale constitutive modeling and numerical simulation of fabric material. International Journal of Solids and Structures, 43 (2), pp. 206-221

[60] Neff P., private communication.

[61] Ogden R.W. Non-linear elastic deformations. New York: Wiley and Sons; 1984.

[62] Ogden R.W., 2003. Nonlinear Elasticity, Anisotropy, Material Stability and Residual stresses in Soft Tissue. CISM Courses and Lectures Series 441, 65-108

[63] Peng X., Guo Z., Du T., Yu W.R., 2013. A Simple Anisotropic Hyperelastic Constitutive Model for Textile Fabrics with Application to Forming Simulation. Composites: Part B, DOI: http://dx.doi.org/10.1016/j.compositesb.2013.04.014

[64] Pietraszkiewicz W., Eremeyev V.A., 2009. On natural strain measures of the non-linear micropolar continuum. International Journal of Solids and Structures 46:3, 774-787

[65] Oshmyan V.G., Patlazhan S.A., Rémond Y., 2006. Principles of structural-mechanical modeling of polymers and composites. Polymer Science Series A 48:9, 1004-1013

[66] Pideri C., Seppecher P., 1997. A second gradient material resulting from the homogenization of an heterogeneous linear elastic medium. Contin. Mech. Thermodyn. 9:5, 241-257

[67] Piola G., 1846. Memoria intorno alle equazioni fondamentali del movimento di corpi qualsivogliono considerati secondo la naturale loro forma e costituzione. Modena, Tipi del R.D. Camera

[68] Placidi L., Rosi G., Giorgio. I., Madeo A., 2013. Reflection and transmission of plane waves at surfaces carrying material properties and embedded in second gradient materials. Mathematics and Mechanics of Solids, DOI: 10.1177/1081286512474016.

[69] Raoult A., 2009. Symmetry groups in nonlinear elasticity: An exercise in vintage mathematics. Communications on Pure and Applied Analysis 8:1, 435-456

[70] Rinaldi A., Krajcinovic K., Peralta P., Lai Y.-C., (2008). Modeling Polycrystalline Microstructures With Lattice Models: A Quantitative Approach. Mech. Mater., 40, 17-36

[71] Rinaldi A. (2009). A rational model for 2D Disordered Lattices Under Uniaxial Loading. Int. J. Damage Mech., 18, 233-57

[72] Rinaldi A., Lai Y.C., (2007), Damage Theory Of 2D Disordered Lattices: Energetics And Physical Foundations Of Damage Parameter. Int. J. Plasticity, 23, 1796-1825

[73] Rinaldi A. (2011). Statistical model with two order parameters for ductile and soft fiber bundles in nanoscience and biomaterials. Phys Rev E , 83(4-2) 046126

[74] Rinaldi A. (2013). Bottom-up modeling of damage in heterogeneous quasi-brittle solids. Continuum Mechanics and Thermodynamics, 25, Issue 2-4, 359-373

[75] Rinaldi A., Krajcinovic D., Mastilovic S., (2007). Statistical Damage Mechanics and Extreme Value Theory. Int. J. Damage Mech, 16:1, 57-76

[76] Rosi G., Madeo A., Guyader J.-L., 2013. Switch between fast and slow Biot compression waves induced by second gradient microstructur at material discontinuity surfaces in porous media. Int. J. Solids Struct., 50:10, 1721-1746

[77] Schröder J., Balzani D., Neff P., 2005. A variational approach for materially stable anisotropic hyperelasticity. Int. J. Solids Struct., 42, 4352-4371

[78] Sciarra G., dell'Isola F., Coussy O., 2007. Second gradient poromechanics, Int. J. Solids Struct, 44:20, 6607-6629

[79] Sciarra G., dell'Isola F., Ianiro N., Madeo A., 2008. A Variational Deduction of Second Gradient Poroelasticity I: General Theory. Journal of Mechanics of Materials and Structures, 3:3, 507-526

[80] Sciarra G., dell'Isola F., Ianiro N., Madeo A., 2008. A Variational Deduction of Second Gradient Poroelasticity I: General Theory, Journal of Mechanics of Materials and Structures 3:3 507-526

[81] Seppecher P., Alibert J.-J., dell'Isola F., 2011. Linear elastic trusses leading to continua with exotic mechanical interactions. Journal of Physics: Conference Series, 319

[82] Spencer A.J.M., Constitutive theory for strongly anisotropic solids, in Continuum Theory of Fibre- Reinforced Composites, CISM International Centre for Mechanical Sciences Courses and Lecture Notes, 282, Spencer A.J. M. Ed., Springer, 1984.

[83] Steigmann, D.J. (1992). Equilibrium of prestressed networks. IMA Journal of Applied Mathematics (Institute of Mathematics and Its Applications), 48:2, 195-215

[84] Steigmann, D.J. (2002). Invariants of the stretch tensors and their application to finite elasticity theory. Mathematics and Mechanics of Solids, 7:4, 393-404

[85] Steigmann, D.J. (2003). Frame-invariant polyconvex strain-energy functions for some anisotropic solids Mathematics and Mechanics of Solids, 8:5, 497-506

[86] Toupin R. 1964. Theories of elasticity with couples-stress. Arch. Rational Mech and Anal., 17, 85-112

[87] Triantafyllidis N., Aifantis E.C.A., 1986. Gradient approach to localization of deformation, I. Hyperelastic materials. J. Elast. 16:3, 225-237

Manuel Ferretti
LaMCoS, Université de Lyon, INSA-CNRS, France & DICEAA, Università dell'Aquila, Italy
20 avenue Albert Einstein, 69621, Villeurbanne cedex, France
e-mail: manuel.ferretti@insa-lyon.fr

Angela Madeo*
LGCIE, Université de Lyon, INSA,
20 avenue Albert Einstein, 69621, Villeurbanne cedex, France
& International research center M&MoCS, Università dell'Aquila, Italy
*: Corresponding author
e-mail: angela.madeo@insa-lyon.fr

Francesco dell'Isola
DISG, Università di Roma "La Sapienza", Italy & International research center M&MoCS, Università dell'Aquila, Italy
e-mail: francesco.dellisola@uniroma1.it

Philippe Boisse
LaMCoS, Université de Lyon, INSA-CNRS, France
20 avenue Albert Einstein, 69621, Villeurbanne cedex, France
e-mail: philippe.boisse@insa-lyon.fr